Chapter 5
Polarization Preservation and Spin Manipulation

Haixin Huang

Abstract In this chapter, we will discuss how the polarization is preserved with real accelerators, including both electrons and protons. In the end, we also present a few examples of spin manipulations.

5.1 Introduction

Before we start, first let us summarize what we have learned so far:

As we learned from previous chapters, spin motion in external electromagnetic fields is governed by Thomas-BMT equation. Spin motion in a synchrotron can be treated with spinors in the form of one-turn matrix of spin. In periodic accelerator structures, spin motion is periodic, which results in the spin tune concept. Because of the periodicity, the spin precession experiences resonant motions. These resonances can be divided into a few categories: imperfection resonances, intrinsic resonances, synchrotron side band resonances, etc. The resonance strength is a function of energy ($G\gamma$), the lattice used (betatron tunes, beta functions), the magnitudes of field errors and orbit errors. They can be calculated with Fourier analysis, by programs such as DEPOL [1]. For an isolated resonance, the final spin can be determined from the initial spin by the crossing speed α and the resonance strength ϵ, using the

H. Huang (✉)
Collider Accelerator, Brookhaven National Laboratory, Upton, NY, USA
e-mail: huanghai@bnl.gov

F. Méot et al. (eds.), *Polarized Beam Dynamics and Instrumentation in Particle Accelerators*, Particle Acceleration and Detection,
https://doi.org/10.1007/978-3-031-16715-7_5

Froissart-Stora formula [2]. The depolarizing resonance is different from betatron resonances where stronger resonances cause more damage. When the adiabatic condition is satisfied, $\frac{|\epsilon|^2}{\alpha} \gg 1$, polarization amplitude can be preserved, by a full spin flip.

A beam bunch is composed of particles with different betatron amplitudes and phases. For an intrinsic resonance, the Froissart-Stora formula needs to be applied to an ensemble of particles with a certain distribution. The most common distribution is Gaussian distribution. Let ε be the Courant invariant of a particle and the distribution function be $\rho(\varepsilon)$. The polarization of the beam after passing through an isolated resonance is given by:

$$< P_f/P_i >= \int_0^\infty (2e^{\frac{-\pi|\epsilon(\varepsilon)|^2}{2\alpha}} - 1)\rho(\varepsilon)d\varepsilon, \quad \rho(\varepsilon) = \frac{1}{2\varepsilon_0}e^{-\varepsilon/2\varepsilon_0}. \tag{5.1}$$

Using the fact that the intrinsic resonance strength is proportional to the square of the particle emittance,

$$|\epsilon(\varepsilon)|^2 = |\epsilon(\varepsilon_0)|^2\frac{\varepsilon}{\varepsilon_0} \tag{5.2}$$

With these conditions, the Froissart-Stora formula for a beam with Gaussian distribution is given as

$$P_f/P_i = \frac{1 - \frac{\pi\epsilon^2}{\alpha}}{1 + \frac{\pi\epsilon^2}{\alpha}}. \tag{5.3}$$

It should be noted that Froissart-Stora formula can only be applied to isolated resonances. The isolated resonance has to satisfy following condition: the distance δ between resonances (assume respective strengths $\epsilon_1,\ \epsilon_2$) is much larger than the resonance strengths. Namely: $\delta \gg \max(\epsilon_1, \epsilon_2)$.

From the Froissart-Stora formula, depending on the resonance strength, there are two ways to preserve polarization through a depolarizing resonance. Very fast crossing applies when $\pi|\epsilon|^2/(2\alpha) \ll 1$, which will result in $P_f/P_i \to 1$. The adiabatic condition applies when $\pi|\epsilon|^2/(2\alpha) \gg 1$, which will result in $P_f/P_i \to -1$.

To maintain the polarization through a resonance, one of two things should happen:

1. strong enough resonance to generate a full spin flip;
2. very fast crossing speed so no or negligible depolarization effect.

In almost all cases we will discuss in this chapter, the isolated resonance condition is satisfied.

5.2 Overcome Resonances by Reducing Their Effects

This section reviews various techniques used to overcome depolarizing resonances by reducing their effects.

5.2.1 Harmonic Orbit Correction

Since the imperfection resonance strength is proportional to the error harmonic of the closed orbit (Sect. 2.3.5.1), by introducing the specific vertical harmonic orbit correction, the resonance can be compensated so that the total resonance strength is either zero or strong enough to fully flip the spin. This method has been used by many accelerators such as Brookhaven AGS [3], KEK [4], KEK Booster [4], Saturne [5] and COSY [6]. There are drawbacks of this method. It is tedious, and the optimal setting could change with time and the tuning of the ring has to be redone. This is a problem if many resonances need to be corrected.

Consider the AGS Booster as an example. In the AGS Booster, the polarized proton beam comes in at $G\gamma = 2.18$ and normally is extracted at $G\gamma = 4.5$. The vertical tune is set at 4.9 to avoid the intrinsic resonance at $0 + \nu_y$ in the Booster. There are two imperfection resonances in the energy range at $G\gamma = 3$ and 4. They both are corrected by the harmonic correction: $G\gamma = 3$ resonance is corrected by compensating the resonance strength to zero and $G\gamma = 4$ resonance is corrected by introducing a full spin flip with strong harmonic orbit component. In the case of $G\gamma = 4$, the resonance strength is enhanced instead. This is possible because $G\gamma = 4$ resonance itself is strong enough that a modest corrector strength can enhance it to get a full spin flip.

For a given corrector current, the effective resonance strength is the combination of both the original imperfection resonance and the corrector resonance strengths. Namely, the Froissart-Stora formula takes the form

$$P_f = P_i(2\exp[\frac{-\pi|\epsilon_1 - \epsilon_2|^2}{2\alpha}] - 1), \tag{5.4}$$

where ϵ_1 and ϵ_2 are the resonance strengths of the original imperfection resonance and the one introduced by the correctors. The resonance strength is a complex number, it has real and imaginary parts or two orthogonal components: cosine and sine (Eq. (2.29)). At proper current of the two orthogonal components, the effective resonance strength is zero and polarization is fully preserved in this case. Since we are going to scan the corrector current, we rewrite the above formula in a slightly different form:

$$P_f = P_i(2\,e^{\frac{-\pi(I_s - I_{s0})^2}{2\sigma_s^2}} e^{\frac{-\pi(I_c - I_{c0})^2}{2\sigma_c^2}} - 1), \tag{5.5}$$

where I_s (I_c) is the corrector current for sine (cosine) component, I_{s0} (I_{c0}) is the sine (cosine) corrector current corresponding to the optimized polarization, and σ_s (σ_c) will provide the width of the sine (cosine) current scan, or sensitivity of the current variation. During the current scan, only one component, either I_c or I_s, is varied. The other component needs to be set as a constant. In other words, the fitting is done with the following format for cosine and sine components separately:

$$P_f = p_0(2e^{\frac{-\pi(I-p_1)^2}{2p_2^2}} - p_3), \tag{5.6}$$

where p_0, p_1, p_2 and p_3 are the fitting parameters. For the cosine component scan,

$$\begin{aligned} p_0 &= P_i \exp\frac{-\pi(I_s - I_{s0})^2}{2\sigma_s^2}, \\ I - p_1 &= I_c - I_{c0}, \\ p_2 &= \sigma_c, \\ p_3 &= 1/\exp[\frac{-\pi(I_s - I_{s0})^2}{2\sigma_s^2}] \end{aligned} \tag{5.7}$$

The terms related to the sine component are absorbed into the fitting parameters.

Exercise 2 (Sect. 5.6) addresses the matching of experimental data using Eq. (5.6).

5.2.2 Speedup the Crossing Speed

The crossing speed can be increased in several ways. The maximum acceleration rate for a beam in a synchrotron is usually set by engineering limits on the maximum achievable ramp rate of the main dipole current and field, so typically increasing the acceleration rate is not an option. The options to increase the crossing speed include rapidly changing betatron tunes over one or a few orbit turns (tune jump); changing radius rapidly while keeping main magnet field constant (radial jump). A complete resonance crossing speed is given in the presence of tune jump:

$$\alpha = G\frac{d\gamma}{d\theta} \pm \frac{dv}{d\theta} \tag{5.8}$$

The crossing speed can be changed by acceleration speed, radial shift (RF manœuver) and rapid tune jump.

5.2.3 Radial Jump

In the case that magnet ramping speed is limited but the RF system is powerful enough, the energy can be quickly changed by shifting the radius while maintaining the main magnet field constant. It is called energy-jump method. An experiment was carried out at the AGS to demonstrate the idea [7]. In the presence of a solenoidal partial snake, a strong coupling is introduced, which in turn generates coupling resonances. The energy jump method was used to cross the coupling resonance near intrinsic resonance $0 + \nu_y$, at $0 + \nu_x$ (a horizontal resonance which is excited in the presence of solenoidal partial snake). The energy-jump was accomplished by rapidly changing the beam circumference by 88 mm using the powerful AGS RF system over 40 turns. Due to the momentum spread, not all the beam particles are crossing the resonance during the jump unless the jump timing is centered. The polarization was measured as function of the jump time T_{jump}. As shown in Fig. 5.1, the final polarization is optimized when the jump time is centered at the resonance $0 + \nu_x$.

5.2.4 Tune Jump (Both Fast and Benign)

The tune jump can be achieved by using pulsed quadrupoles to rapidly shift the tune and thus make the resonance crossing rate α very large. This method has been applied in AGS [3], KEK, KEK Booster[4], COSY[8] and other accelerators. The mechanism of the tune jump is illustrated in Fig. 5.2.

In the AGS, the rapid tune shifts were produced by special fast quadrupole magnets; ten quadrupoles were installed in ten of the twelve superperiods. Sophisticated power supplies, which generated pulses with a maximum output of 2250 A at 15 000 V, were connected to 10 of these quadrupoles. The field in each fast quadrupole had a 1.6 μs rise time and then decayed back to zero in about 3 ms. Each quadrupole had a maximum field gradient of 11.7 kG/m. The AGS revolution time is in the order of 3 μs, and this fast tune jump is a one turn tune jump. It can generate a tune jump in the order of 0.2 unit in one orbit turn. One example of the tune jump effect on polarization is shown in Fig. 5.3. When the jump timing is centered at the intrinsic resonance, the polarization is maximized. The plateau of polarization means there is a tolerance of 0.1 GeV/c for the jump timing.

The major problem of the fast tune jump is the emittance growth due to the large and fast tune jump: non-adiabatic excitation of quadrupoles will generate emittance growth due to the non-adiabatic excitation of closed orbit and the non-adiabatic betatron amplitude mismatch. This is especially true if the center of the closed orbit does not coincide with the center of the tune jump quadrupoles. Closed orbit oscillations arising from the non-adiabatic dipole fields in tune jump quadrupoles will generate emittance growth. Efforts were made to center tune jump quadrupoles in the AGS and the emittance growth was greatly reduced [9]. Experimental tests in

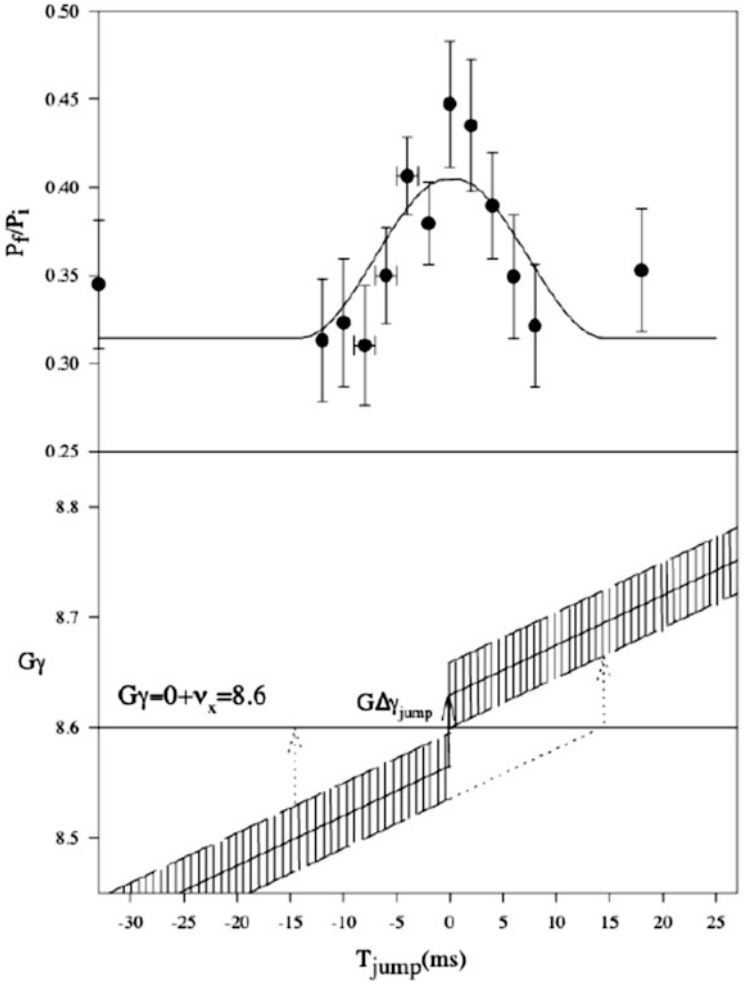

Fig. 5.1 Radial jump scheme and polarization gain with the jump. The hash lines represent the beam with a certain momentum spread

1990s showed that the single turn tune jump can be further relaxed to multiple turns (20–30 turns). The emittance growth in this case is further reduced [7].

These tune jump quadrupoles eventually were removed from AGS after AGS polarization preservation switched to strong partial snakes (see below). However, a new type of resonance, so-called horizontal intrinsic resonances [10], gives this method a new life. In the presence of strong partial snakes, the stable spin direction is not vertical. Therefore the perturbing fields that rotate the spin away from the stable direction have vertical as well as horizontal components. Particles undergoing horizontal betatron oscillations encounter vertical field deviations at the horizontal

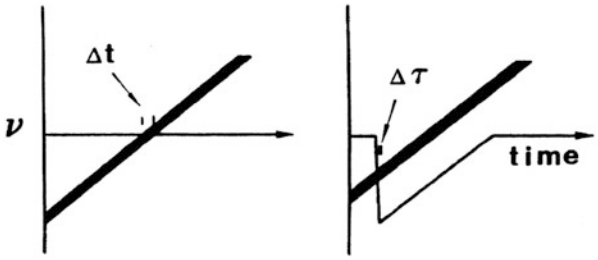

Fig. 5.2 Tune jump scheme illustration. The beam energy is shown as a thick line (to include the momentum spread) and the intrinsic resonance is represented by the horizontal line with arrow in the left plot. On the right plot, the resonance curve is shown along with the fast tune shift due to the pulsed quadrupoles. The resonance crossing time is greatly reduced from Δt to $\Delta\tau$

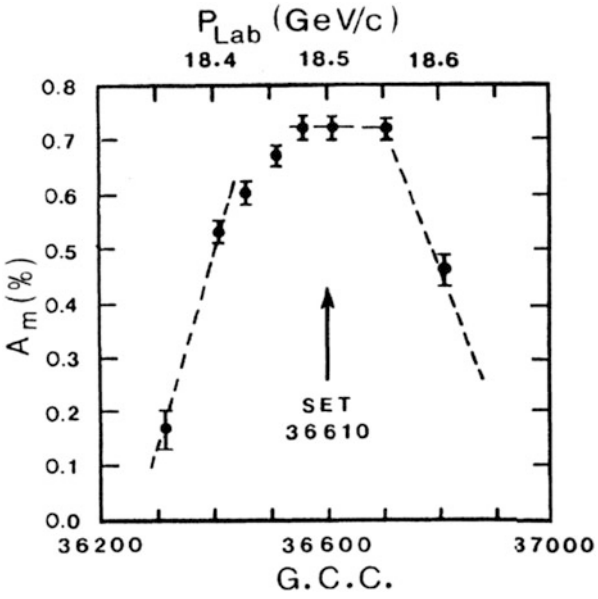

Fig. 5.3 The measured asymmetry (proportional to polarization) is plotted vs. the tune jump firing energy in unit of Gauss Clock Counts (GCC). For a given radius, the beam energy is proportional to the beam momentum. The GCC is converted to momentum at the top of the figure

oscillation frequency. As a result, resonances are driven by the horizontal betatron oscillations, and will occur whenever the spin tune satisfies $\nu_{sp} = k \pm \nu_x$. This type of resonance is called horizontal intrinsic resonance. Since the two partial snakes are helical dipole magnets, the vertical magnetic field deviations distributed along the snakes are the main parts of the polarization perturbation. They have been observed in the AGS [10] (Fig. 5.4).

These resonances in general are weak but they are numerous. For an RMS emittance of $2\,\mu$m, the resonance strength is in the order of 10^{-5} to 10^{-4}, but

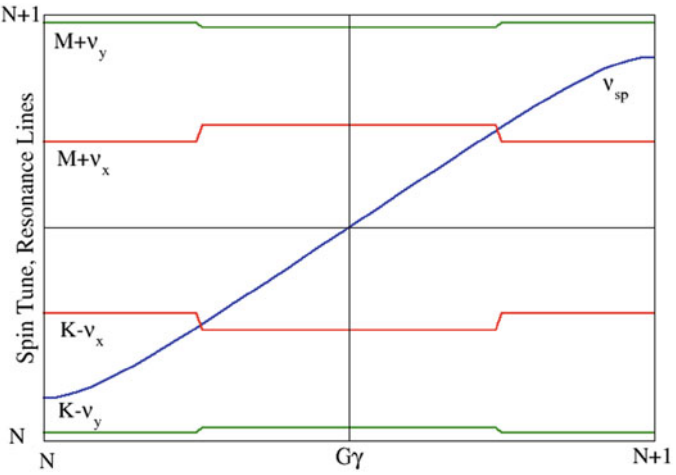

Fig. 5.4 The schematics of tune jump scheme. The blue trace is the spin tune as a function of $G\gamma$ during the acceleration. The red lines are the horizontal intrinsic resonance lines. The green lines are vertical intrinsic resonance lines. Over one unit of $G\gamma$, two horizontal intrinsic resonances are crossed. M, K, and N are integers

there are over seventy of them! Given the AGS nominal ramp rate, a tune jump of 0.04 in 100 μs should work. This increases the crossing speed by about 4 times. Maintaining the adiabaticity of the particle motion is the key to minimize any emittance growth, even for a small tune jump. A tune jump adiabatic enough to produce negligible emittance growth is sometimes called "benign". A pair of tune jump quads were installed in straight sections in two adjacent superperiods in the AGS, I5 and J5, where the β_x is at its maximum. It should be noted that the vertical tune would also be affected by the tune jump quads, but at a small amplitude due to the small beta function. As the vertical tune is fairly close to integer ($\nu_y \sim 8.98$), the perturbation to orbit motion needs to be minimized. Figure 5.5 shows the betatron tune measurements along the energy ramp. The tune measurement time was chosen such that it gave tunes alternatively as jump up value and jump down value (or no jump value). The ramp starts at 149 ms and reaches flattop at 581 ms. The figure shows that the horizontal tune jump amplitude is about 0.04 and the vertical tune jump amplitude is about 0.02.

Figure 5.6 illustrate the resonance crossing with tune and energy spreads. They are plotted for resonances near $G\gamma = 45$, but are representative for all resonances when $G\gamma > 19$. To benefit from the tune jump, the beam particles have to cross the resonance line during the jump. For the given beam parameters (tune jump amplitude, chromaticity, beam momentum spread), about 76% beam will benefit from the tune jumps above $G\gamma > 19$. The jump timing determination requires accurate determination of beam energy as function of ramp time. The beam energy information on the energy ramp comes from measuring the AGS main magnetic field and measuring the beam momentum offset using the radial average from the

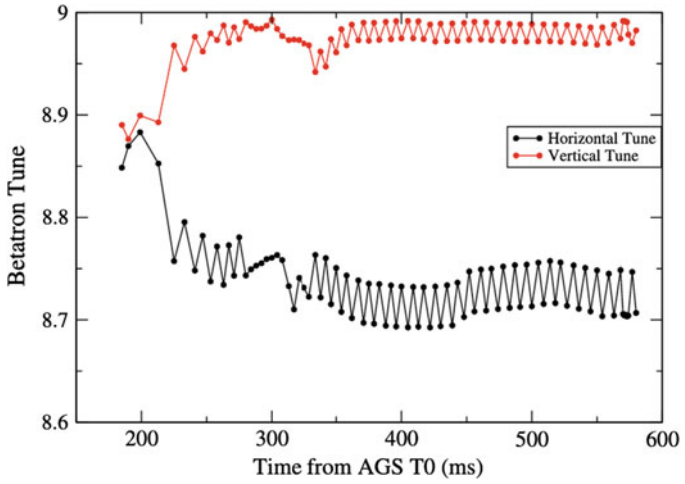

Fig. 5.5 The measured betatron tunes along the ramp as a function of time from AGS T0. Note that there was no tune jump around 300 ms to avoid interference with other beam operation system

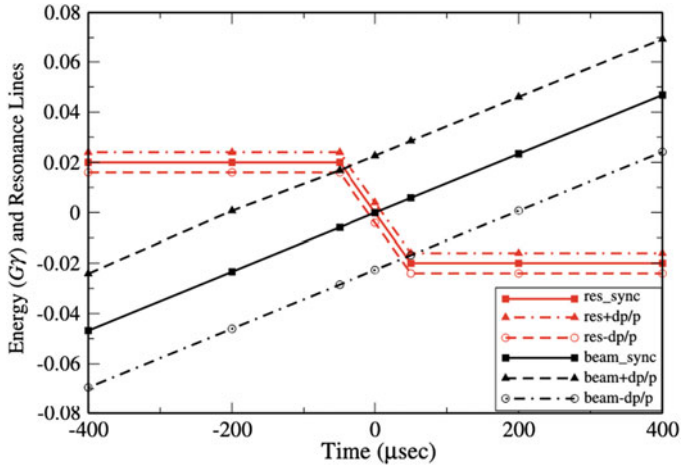

Fig. 5.6 Sketch of a resonance crossing on the increasing ν_x side of the pulse ($G\gamma = 54 - \nu_x = 45.3$). The horizontal axis is relative time to the resonance crossing. The vertical axis is energy relative to the synchronous particle at jump time in units of $G\gamma$. The solid line applies to the synchronous particle, and the two types of broken lines apply to the boundary particles at the FWHM. The momentum FWHM width is assumed as 10^{-3}, which is close to the real dp/p in the later part of the ramp. A chromaticity of -8 is used for the plot. The ramp rate $dG\gamma/dt$ is 0.117/ms. The plot shows that particles within FWHM (76 % of the beam) benefit from the tune jump

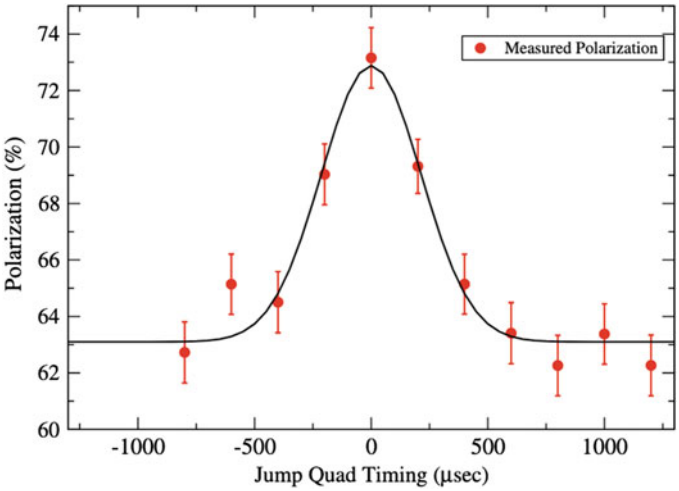

Fig. 5.7 The measured polarization at the AGS extraction as a function of overall jump quad timing. Error bars are statistical errors only. The solid line is a fit of Gaussian distribution with $\sigma = 214\,\mu s$

beam position measuring system. As a cross check, the second set of beam energy information is derived from beam frequency and path length. The jump timing is then derived from the beam energy and horizontal tune as a function of the ramp time.

Since the polarization loss from an individual resonance is too small to measure, it is only practical to do the overall timing scan to check the effect of tune jump on the polarization (Fig. 5.7). With the assumption of Gaussian beam distribution, the polarization distribution is expected to be Gaussian. From the beam parameters, the width of this Gaussian is expected to be around 145 μs. If there are errors in the individual jump quad timing, the distribution σ will be larger, which is what has been observed.

In summary, the tune jump method is very powerful to overcome intrinsic resonances. The associated emittance growth requires centering the beam orbit inside the jump quads. When the tune jump speed can be relaxed to 20–30 turns, the emittance growth is manageable at a few percents level. This method is still in use such as the AGS horizontal tune jump system [11] and it is also planned for the future EIC polarized deuteron program [12].

5.2.5 *Fast Acceleration for Weak Resonance*

The intrinsic resonance condition is given as $\nu_{sp} = nP \pm \nu_y$. If the superiodicity P can be increased in the lattice design stage, the space between strong intrinsic

resonances can be increased. It is possible that the resonance condition for strong intrinsic resonances are pushed out of a given energy range. Specifically, for $P > \nu_y$, the first two important intrinsic resonances occur at $G\gamma = \nu_y$ and at $G\gamma = P - \nu_y$. If we now ensure that both ν_y and $P - \nu_y$ are greater than the maximum $G\gamma$ value then all the major intrinsic spin resonances can be avoided. Alternatively, one could also choose ν_y to be greater than the maximum $G\gamma$ and $P - \nu_y$ less than the lowest $G\gamma$ value. This ingenious optical design has been used in the EIC RSC ring design [13]. By choosing $P = 96$ and integer part of the vertical betatron tune to be $41 < [\nu_y] < 55$, polarized beam can be accelerated to $G\gamma = 41$ from low energy without crossing a strong intrinsic resonance. Here $[\nu_y]$ indicates the nearest integer to the vertical betatron tune.

Unfortunately, the existing RHIC tunnel resembles a hexagon with rounded corners rather than a circle, and therefore has a natural periodicity of six. However, if we consider that the spin precession, which advances as $G\gamma$, occurs in the dipoles and does not advance at all in a drift, one can recover the periodicity of 96 from the point of view of $G\gamma$ precession. This can be accomplished by designing the straight sections such that their betatron phase advance is equal to $2\pi k$ with $k \in \{1, 2, 3, ...\}$. In this way the straight sections will not contribute to the integral which defines the strength of the spin resonance (see Fig. 5.8). Thus the 96 periodicity can be maintained from the point of view of the spin precession. High periodicity arcs are used and unity transformation in the straight sections are used to transform the ring to the hexagon shape of RHIC tunnel. This suppresses all systematic depolarizing resonances up to $G\gamma$ =41.

The RCS is designed to eliminate intrinsic spin resonances during the acceleration cycle. However, any deviation from this ideal geometry, whether intentional, like insertion regions or accidental, like survey errors, has the potential to spoil the symmetry that keeps all the intrinsic resonance strengths sufficiently low. By minimizing the contributions to the spin integral introduced by these insertions we can ensure that polarization is maintained to emittances well beyond foreseeable

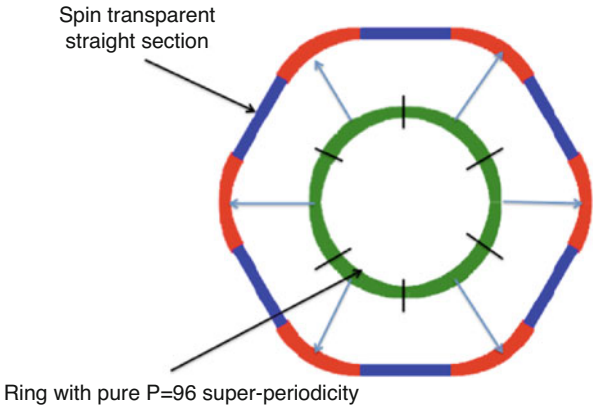

Fig. 5.8 Projecting the pure ring lattice with 96 periodicity onto the RHIC sixfold periodic ring

operational conditions. The results in Fig. 5.9, show that for the slowest ramp time of 200 ms 94% polarization transmission can be achieved.

5.2.6 *Full Siberian Snake*

The snake magnet concept was first introduced by Russian physicists S. Derbenev and A.M. Kondratenko and the trajectory inside the magnet is like a snake (as shown in Fig 5.10). The idea is simple but genius: the spin is rotated by 180° around an axis in the horizontal plane. Any perturbation to the spin before the snake is unwounded by similar perturbation in the following section or orbit turn. For this reason, full snake is put into the category of overcoming resonances by reducing their effects. Because of the Siberian origins of the idea and the serpentine shape of the particle

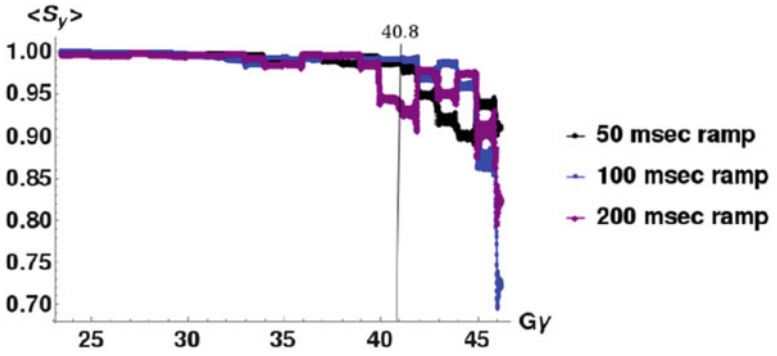

Fig. 5.9 ZGOUBI tracking results for 8 particles at 1000 mm-mrad normalized emittance. Comparing ramp times 50–200 ms. The vertical axis $\langle S_y \rangle$ represents the average vertical components of the spin vector. The vertical line marks the location of $G\gamma = 41$

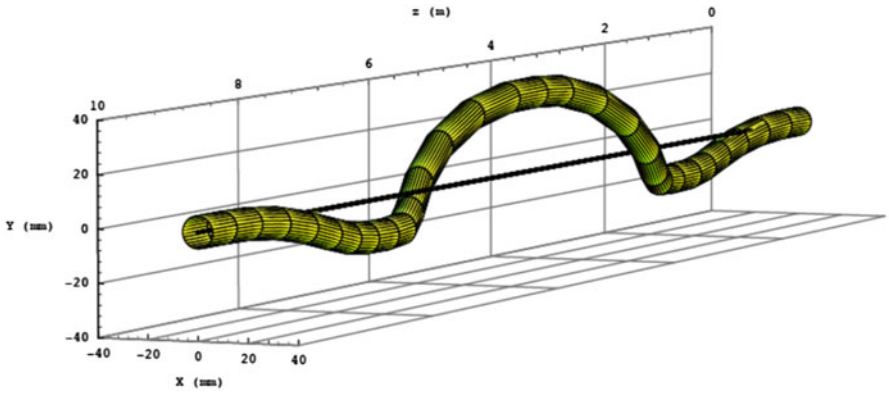

Fig. 5.10 Three-dimensional view of the trajectory through a RHIC Snake

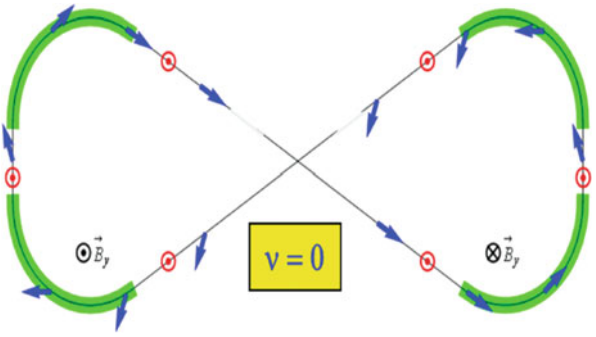

Fig. 5.11 Schematics of the figure-8 ring principle. The red and blue arrows are possible spin components in the ring: vertical or horizontal. With two identical halves of the ring except for the dipole magnet fields which are reversed, the perturbation to spin motion in the two half rings are compensated

trajectory, these magnets were dubbed Siberian snakes by Ernest Courant. In RHIC, dual full snakes are separated by half of the ring. Each snake rotates the spin vector 180° around an axis in the horizontal plane. There are two consequences of two snakes. First the stable spin direction of the whole ring is vertical. Second, for two snakes with the axis perpendicular to each other, spin tune is 0.5.

In the presence of snakes, one would think that the polarization can be preserved. However, there are additional high order depolarizing resonances, called snake resonances [14]. The snake resonance condition is given as

$$m\nu_y = \nu_{sp} + k \tag{5.9}$$

where m and k are integers. m is called the snake resonance order. Examples of the resonance conditions are $5 \times 0.7 = 0.5 + 3$ for $\nu_y = 0.7$; $2 \times 0.75 = 0.5 + 1$ for $\nu_y = 0.75$. For two snakes in a synchrotron, the even order resonances do not exist if the closed orbit is fully corrected, but the odd order resonances do. In the RHIC operation, there is almost no polarization loss on the ramp below 100 GeV, about 10%–15% polarization loss between 100 and 255 GeV [15].

Another idea similar to the snake is the figure-8 ring (Fig. 5.11). The perturbation to the spin motion in a figure-8 ring is also compensated in the two half rings, because the magnetic fields reverse signs [16].

5.3 Resonance Enhancement Method

As the Froissart-Stora formula shows, with strong enough resonance strength, the spin can be fully flipped when crossing the resonance adiabatically. Polarization is preserved as the result. Options to enhance the resonance strength include running an AC dipole to enhance the intrinsic resonances and running a partial snake to enhance imperfection resonances. When the partial snake strength is strong enough, it can also overpower the intrinsic resonances. In these cases, the two resonances can be made to occur at nearly the same energy by choosing a tune very near an

integer to create overlapping resonances. Condition for overlapping resonances is

$$\delta \ll \min(\epsilon_1, \epsilon_2) \tag{5.10}$$

This condition can be easily satisfied if using partial snake for the imperfection resonance case, as the two resonances are at the exact same location, and $\delta = 0$. From this condition, one can see that AC dipole is not usable for a weak resonance: the required separation is not feasible.

5.3.1 AC Dipole

An AC dipole is a magnet that can be adiabatically excited and de-excited with a continuous sine-wave in order to coherently move circulating beam out to large betatron amplitudes without incurring the emittance blow up. It has also been referred as RF dipole in some references.

Since the intrinsic spin resonance strength is proportional to the betatron amplitude, the final polarization is an ensemble average of the Froissart-Stora formula over the betatron amplitude of the beam particles. It is difficult to achieve a full spin flip for all particles since the resonance strength of the beam core is small. Alternatively, if the beam is kicked to induce a coherent betatron oscillation so that the betatron oscillation amplitudes of all particles are large, a full spin flip can be attained [17]. Essentially, the AC dipole field and the focusing potential of the accelerator form a potential well that preserves the emittance of the beam. Such a controlled coherent betatron oscillation can be obtained by using an AC dipole magnet operating at a frequency close to a betatron sideband. The schematics of the method is shown in Fig. 5.12. There are two requirements to use the AC dipole. First, there should be a large enough physical aperture for the needed large betatron motion amplitudes. Second, the original intrinsic resonance strength needs to be strong enough that the needed artificial resonance strength can be achieved with feasible tune separation. To preserve the emittance, the AC dipole amplitude was ramped up and down adiabatically. The drive signal and the measured beam position signals from the AGS AC dipole are shown in Fig. 5.13.

In a linear approximation, the amplitude of the coherent betatron motion is given by

$$y_{coh} = \frac{B_m l}{4\pi(B\rho)\delta}\beta_y \tag{5.11}$$

where $B_m l$ is the integrated field of the AC dipole, $B\rho$ is the magnetic rigidity of the beam, β_y is the vertical betatron function at the AC dipole, and δ is the difference between the AC dipole tune and the tune of the nearest betatron sideband. Equation 5.11 shows that although the coherent amplitude is larger with smaller tune separation δ, the beam is unstable at $\delta = 0$. Figure 5.14 shows the measured

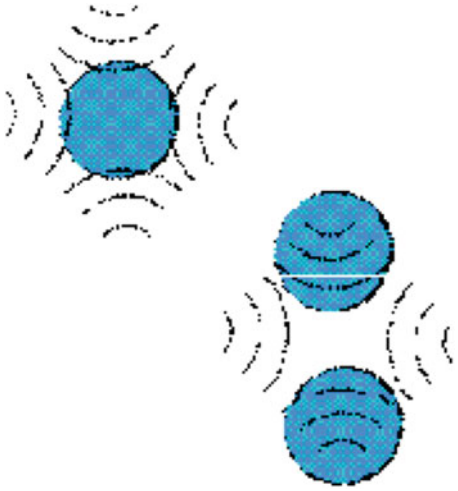

Fig. 5.12 Beam in a quadrupole with and without AC dipole. The dash lines are the magnetic fields of the quadrupole. Left: beam stays in the center of the quadrupole and particles experience different magnetic fields. Right: the whole beam experiences large enough betatron amplitudes which results in full spin flip

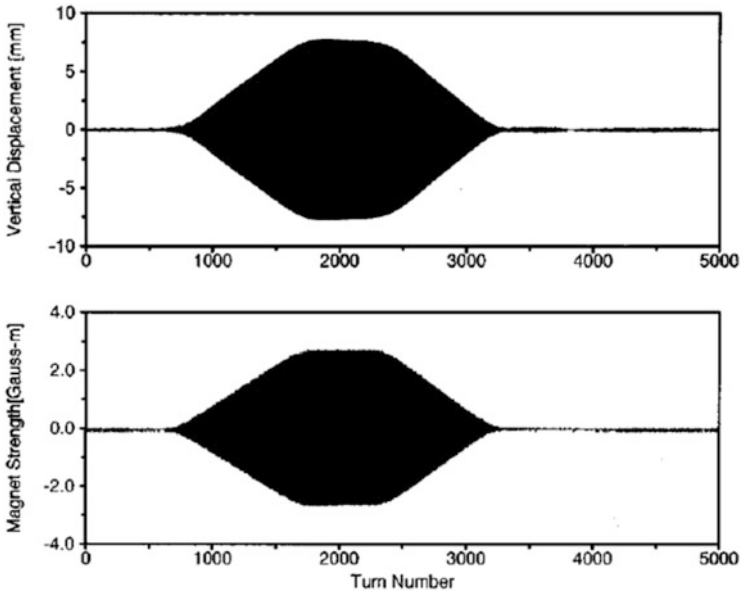

Fig. 5.13 Transverse displacement from BPM (top) and the AC dipole magnet field amplitude (bottom) as a function of turn number of AGS

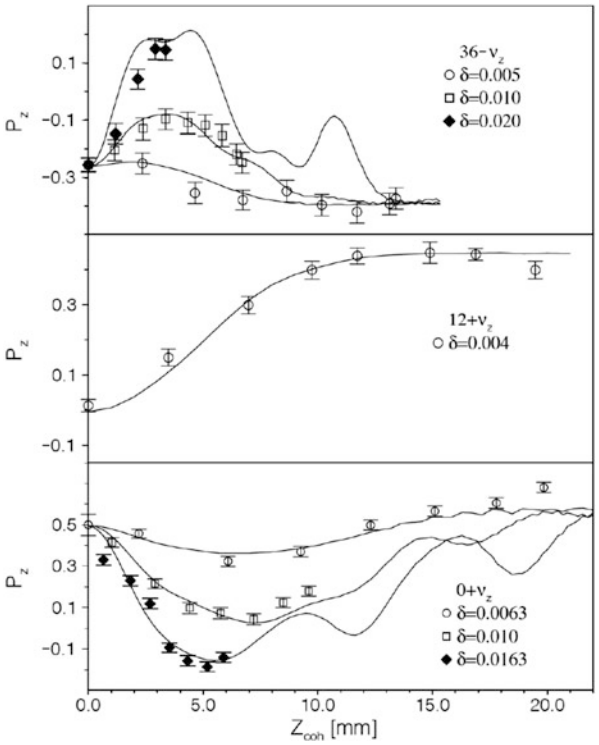

Fig. 5.14 Measured proton polarization vs the coherent betatron oscillation amplitude for different tune separations at spin depolarizing resonances $0 + \nu_y$ (bottom plot), $12 + \nu_y$ (middle plot), and $36 - \nu_y$ (upper plot). P_y stands for the vertical polarization, while Y_{coh} stands for the vertical coherent oscillation amplitude (Note that in Bai et al. [18] notations, vertical axis y is denoted by z). The error bars show only the statistical errors. The resonance strength of the coherent spin resonance due to the AC dipole is proportional to the coherent betatron amplitude. The lines are the results of multi-particle spin simulations based on a model with two overlapping spin resonances

polarization at three energies versus the AC dipole strength, which is converted to the corresponding coherent betatron amplitude [18]. The lines shown on the figure correspond to results obtained from numerical spin simulations of a two spin resonance model. The oscillatory behavior of the simulation result is due to the interference between the coherent betatron oscillations and the intrinsic betatron motion. The spin vector of each particle was tracked by multiplying its turn by turn transform matrix. The beam polarization was then obtained from the spin ensemble average of a Gaussian beam distribution. The agreement between experimental data and simulations are very good.

5.3.2 Partial Snake for Imperfection Resonances

Partial snake is a device to rotate the spin by an angle $\phi_{\rm sp}$ less than 180° in one orbit turn. Such a spin rotator can be constructed by using either solenoidal magnets, or a sequence of interleaved horizontal and vertical dipole magnets producing only local orbit distortions. For low energy synchrotrons like the Brookhaven AGS with weak depolarizing resonances, one might consider solenoidal snake. However, for practical field strengths, a full solenoidal snake would require 10 m of straight section, which is not available in the AGS. Strong solenoids can also cause undesirable coupling between horizontal and vertical betatron oscillations, which would require compensation to maintain beam stability. Another option is to use helical dipole as snake. The required magnet field is not practical to be ramped quick enough along the energy ramp. For a constant field, the optical distortions at lower energies would reduce the dynamic aperture. With the constraints in the AGS, it is better to overcome the imperfection resonances with a partial snake [19].

To illustrate how a partial snake works, we consider a perfect synchrotron with a solenoidal snake inserted. For an ideal particle (which moves on the betatron closed orbit without displacement) in a perfect synchrotron, where $\xi = 0$, the spinor is transformed according to

$$\Psi(\theta_f) = e^{-\frac{1}{2}iG\gamma[\theta_f-\theta_i]\sigma_3}\Psi(\theta_i) = T(\theta_f,\theta_i)\Psi(\theta_i), \tag{5.12}$$

where θ_i and θ_f are the initial and final orbit angles, respectively. When $\theta_f - \theta_i = 2\pi$, the spinor is transformed by a spin transfer matrix, called one turn map (OTM) [20],

$$T(\theta_i + 2\pi, \theta_i) = e^{-iG\gamma\pi\sigma_3}, \tag{5.13}$$

where the stable spin direction is vertical ($\hat{e}_3$). When solenoidal fields (rotating the spin by $\phi_{\rm sp}$ radian along the longitudinal $\hat{e}_2$ direction) are present, the OTM, T, is obtained as a product of a spin rotation in the Siberian snake by an angle $\phi_{\rm sp}$ around the longitudinal direction and the precession in the main bending magnets around the vertical direction by the angles $G\gamma\theta$ (before the snake) and $G\gamma(2\pi - \theta)$ (after the snake):

$$T = e^{-i\frac{1}{2}G\gamma(2\pi-\theta)\sigma_3}e^{-i\frac{1}{2}\phi_{\rm sp}\sigma_2}e^{-i\frac{1}{2}G\gamma\theta\sigma_3}, \tag{5.14}$$

where θ is the orbit angle between the observation point and the snake. Completeness of Pauli matrices guarantees that any succession of rotations in the 3-D space is equivalent to a rotation around a specified axis. If the spin vector is lying on this direction initially, it will stay on this direction. That is the so-called spin closed orbit. The OTM can be rewritten as a precession around the spin close orbit $\hat{n}_{co}$ (canonical form):

$$T = e^{-i\pi\nu_{sp}\hat{n}_{co}\cdot\boldsymbol{\sigma}}, \qquad \hat{n}_{co} = \cos\alpha_3\hat{e}_3 + \cos\alpha_2\hat{e}_2 + \cos\alpha_1\hat{e}_1, \tag{5.15}$$

where ν_{sp} is the spin tune and $(\cos\alpha_1, \cos\alpha_2, \cos\alpha_3)$ is direction cosine of $\hat{n}_{co}$ along $(\hat{e}_1, \hat{e}_2, \hat{e}_3)$ axes respectively. A spin vector lying along the $\hat{n}_{co}$ is invariant under the transformation of the Eq. (5.15). On the other hand, any spin vector which is not lying along the $\hat{n}_{co}$, will precess around the $\hat{n}_{co}$ at a rate of ν_{sp} precessing turns per revolution around the synchrotron. Identifying matrix elements of Eq. (5.14) with those of Eq. (5.15),

$$\cos\pi\nu_{sp} = \cos\frac{\phi_{\rm sp}}{2}\cos G\gamma\pi \tag{5.16}$$

and

$$\cos\alpha_3 = \frac{1}{\sin\pi\nu_{sp}}\sin(\pi G\gamma)\cos(\frac{\phi_{\rm sp}}{2}), \tag{5.17}$$

$$\cos\alpha_1 = -\frac{1}{\sin\pi\nu_{sp}}\sin G\gamma(\pi-\theta)\sin(\frac{\phi_{\rm sp}}{2}), \tag{5.18}$$

$$\cos\alpha_2 = \frac{1}{\sin\pi\nu_{sp}}\cos G\gamma(\pi-\theta)\sin(\frac{\phi_{\rm sp}}{2}). \tag{5.19}$$

For a 100% snake, $\phi_{\rm sp} = \pi$, we have $\nu_{sp} = 1/2$. Neither resonance condition discussed in Chapter 1 is therefore ever satisfied regardless of the beam energy. For a partial snake, $\phi_{\rm sp} < \pi$, when $\phi_{\rm sp}$ is small, the spin tune is nearly equal to $G\gamma$ except when $G\gamma$ equals an integer n, where the spin tune ν_{sp} obtained from Eq. (5.16) is shifted from the integer by $\pm\phi_{\rm sp}/2$. Thus, the partial snake creates a gap at all integers in the spin tune, and since the spin tune never equals an integer, the imperfection resonance condition is never satisfied. Thus the partial snake can overcome all imperfection resonances, provided that the existing resonance strengths in the lattice are much smaller than the gap created by the partial snake. The denominator in Eqs .(5.17)–(5.19) can be calculated from Eq. (5.16):

$$\sin\pi\nu_{sp} = \pm\sqrt{1-\cos^2(\pi G\gamma)\cos^2(\phi_{\rm sp}/2)}. \tag{5.20}$$

The physics constraint is that the change of the stable spin direction has to be continuous with $G\gamma$. Due to the gap $\pm\phi_{\rm sp}/2$, $\sin\pi\nu_{sp}$ is not continuous when changing the sign. So we should choose positive root in Eq. (5.20). The Eqs. (5.17)–(5.19) can be rewritten as

$$\cos\alpha_3 = \frac{1}{\sqrt{1-\cos^2(\pi G\gamma)\cos^2(\phi_{\rm sp}/2)}}\sin(\pi G\gamma)\cos(\frac{\phi_{\rm sp}}{2}) \tag{5.21}$$

$$\cos\alpha_1 = -\frac{1}{\sqrt{1-\cos^2(\pi G\gamma)\cos^2(\phi_{\rm sp}/2)}}\sin G\gamma(\pi-\theta)\sin(\frac{\phi_{\rm sp}}{2}), \tag{5.22}$$

$$\cos\alpha_2 = \frac{1}{\sqrt{1-\cos^2(\pi G\gamma)\cos^2(\phi_{sp}/2)}}\cos G\gamma(\pi-\theta)\sin(\frac{\phi_{sp}}{2}). \quad (5.23)$$

The effect of a partial snake can also be analyzed in another view. The localized spin rotation by a partial snake is

$$\phi_{sp}\delta(\theta-\theta_0)$$

and the strength of generated resonance is the Fourier amplitude:

$$\frac{\phi_{sp}}{2\pi}e^{in\theta_0} \quad \text{for all } G\gamma = n.$$

This means that the spin rotator is equivalent to imperfection resonances at all integer harmonics with equal resonance strengths. With the presence of an imperfection resonance and a partial snake, the Froissart-Stora formula can be rewritten as

$$\frac{P_f}{P_i} = 2\exp(-\frac{\pi}{2\alpha}|\epsilon + \frac{\phi_{sp}}{2\pi}e^{in\theta_0}|^2) - 1. \quad (5.24)$$

Complete spin-flip occurs if

$$\phi_{sp} \gg 2\pi|\epsilon| + \sqrt{8\pi\alpha}.$$

For the AGS, $\alpha = 4.5\times10^{-5}$, $|\epsilon| < 0.01$ from previous experiment [3, 9], thus $\phi_{sp} = 0.05\pi$ is enough to overcome all imperfection resonances. Then the spin dynamics when crossing the imperfection resonances will be dominated by the partial snake.

The experiment of a partial snake was carried out in the AGS [21]. Figure 5.15 shows the measured polarization as a function of $G\gamma$ for a 10% partial snake. The polarization was observed to follow the predicted spin flip in passing through each imperfection resonance without loss of polarization. Without the snake, shown as open circles, there was some depolarization at $G\gamma = 8$. The increased depolarization when $G\gamma$ is slightly larger than an integer, particularly noticeable for $G\gamma = 8$, is due to the reduced acceleration rate just before the polarization measuring flat top. With the partial snake to overcome the imperfection resonances, the polarization is maintained through the imperfection resonances at $G\gamma$ =integers, but there are losses at intrinsic resonances. Without the partial snake, polarization is lost after $G\gamma = 12.5$ as shown in Fig. 5.16.

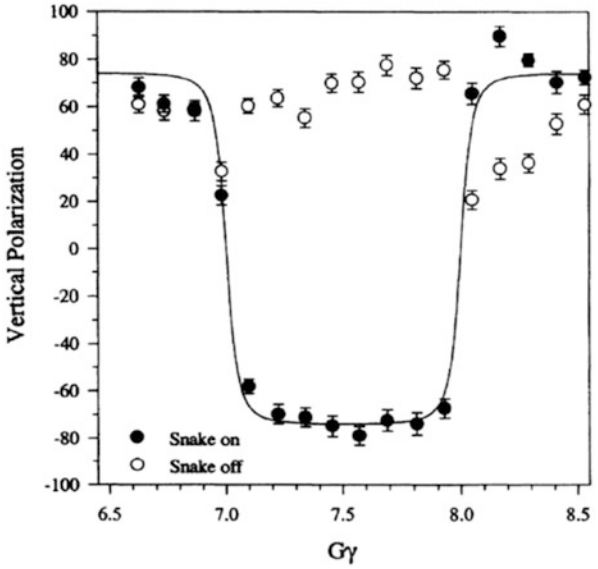

Fig. 5.15 The measured vertical polarization as a function of the spin tune $G\gamma$ for a 10% snake is shown with and without a partial snake. Note that partial depolarization at $G\gamma = 8$ is avoided by using a 10% snake. The error bars only represent the statistical errors. The solid line is the result of Eq. (5.22). The measurement was done at betatron tunes of $\nu_x = 8.7$ and ν_y=8.8

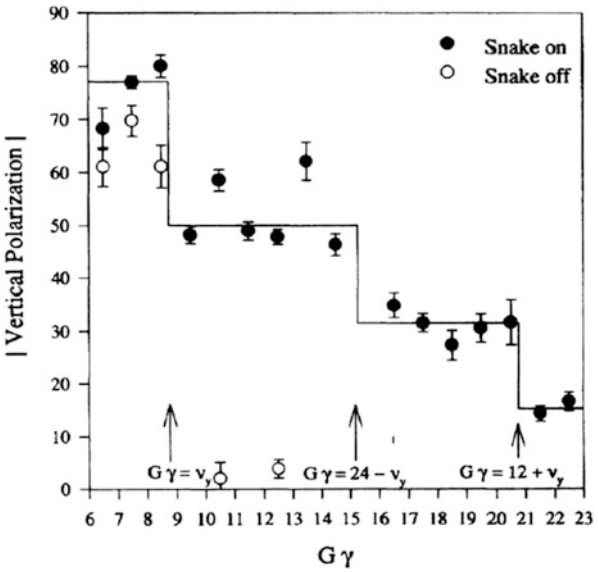

Fig. 5.16 The measured absolute value of the vertical polarization at $G\gamma = n \pm \frac{1}{2}$, up to $G\gamma = 22.5$ (solid points). Note that partial depolarization is due to intrinsic spin resonances at $G\gamma = 0 + \nu_y, 24 - \nu_y$ and $12 - \nu_y$

5.3.3 *Strong Partial Snake to Overcome Intrinsic Resonances*

For a full snake, the spin tune is 1/2 for all energies, the spin tune gap is 0.5. A strong partial snake generates large spin tune gap for $G\gamma = N$, where N is an integer. When the gap is large enough to put the vertical tune inside the spin tune gap, the intrinsic resonance condition can never be satisfied. Then it can overcome both intrinsic and imperfection resonances. The spin tune gaps for various partial snake strengths are shown in Fig. 5.17. Alternatively, this can be understood by a strong resonance at $G\gamma = N$ which overpowers the nearby imperfection and intrinsic resonances.

An experiment was carried out in the AGS with the solenoidal partial snake [22]. At low energies, the magnet can generate a stronger partial snake. The experiment was carried out to overcome $0 + \nu_y$ resonance located near $G\gamma = 8.7$ with solenoid magnet running as an 11.4% partial snake. The polarization was measured at $G\gamma = 12.5$. The results are shown in Fig. 5.18. Note that with a strong snake, the stable spin detection will deviate from vertical significantly. For example, it will be 18° for a 20% partial snake.

As shown in Fig. 5.18, the measured polarization reached a plateau when the vertical betatron tune was very close to 9.00. The polarization loss in this region was only about 6% and can be completely explained by spin mismatching at AGS injection and depolarization from coupling resonances as discussed below.

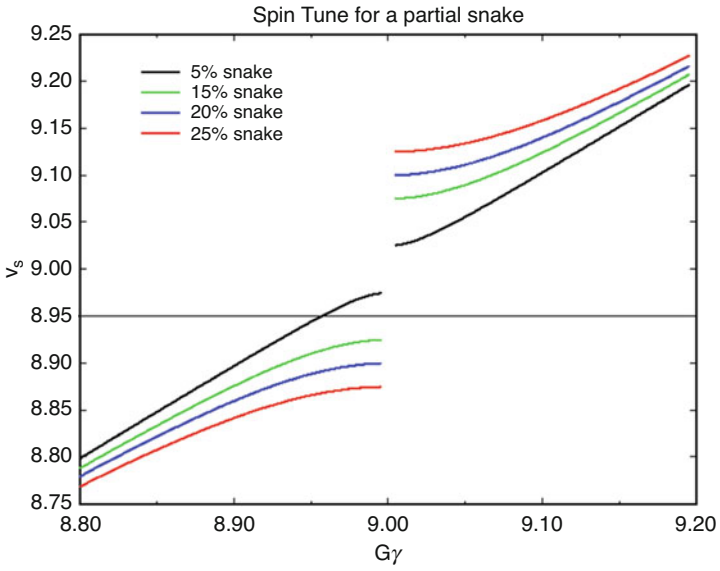

Fig. 5.17 Spin tune for various partial Siberian snake strengths. The straight line indicates a possible value for the vertical betatron tune

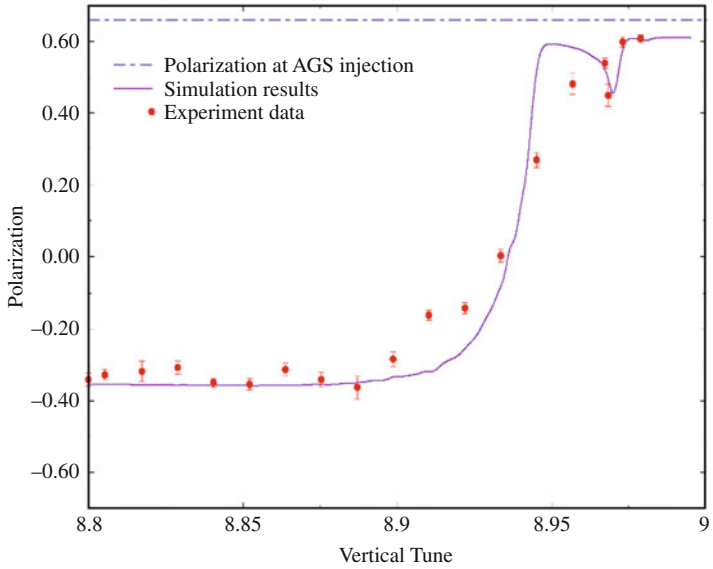

Fig. 5.18 The measured vertical polarization as a function of the vertical betatron tune for an 11.4% partial Siberian snake. The dashed straight line indicates the polarization level measured at the end of the linac. Since the two imperfection resonances in the Booster have been corrected by harmonic orbit correctors, this is also the beam polarization at AGS injection. The solid curve shows the results of both multi-particle simulations and DEPOL calculations

These observations agree well with spin dynamics calculations.With a partial Siberian snake inserted, there are two strong resonances in this energy region: one located at $G\gamma = 9$ generated by the partial Siberian snake and the intrinsic resonance at $G\gamma = 0 + \nu_y$. When the intrinsic and artificial resonances do not overlap ($\nu_y \leqslant 8.85$), the resonance at $G\gamma = 9$ should flip the spin completely while the intrinsic resonance at $G\gamma = 0 + \nu_y$ causes some depolarization. When the two resonances are very close, such as for $\nu_y = 8.98$, the intrinsic resonance is overpowered by the resonance at $G\gamma = 9$. The particles essentially just experience one resonance at $G\gamma = 9$, and full spin flip is observed. When the two resonances are at intermediate separations, such as for $\nu_y \approx 8.90$ to 8.95, they interfere with each other.

Since there is linear coupling between the beam motion in the two transverse planes, the following coupling resonances in the vicinity of $G\gamma = 9$ should also be considered: $G\gamma = 17 - \nu_x, 0 + \nu_x, 18 - \nu_x$, and $1 + \nu_x$. These resonances are not in the spin-tune gap generated by the strong partial snake. Since ν_x and ν_y are well separated, these resonances can be treated separately as isolated resonances. Using the Froissart-Stora formula, the total polarization loss due to the coupling resonances was calculated to be 5%. The polarization loss due to spin mismatching at injection was calculated to be 1%. The difference of the injection polarization and the measured one at $G\gamma = 12.5$ is well understood.

5.3.4 Dual Partial Snakes

For a strong partial snake, however, polarization loss due to spin mismatch at injection and extraction is no longer negligible. A 20% snake will lead to a 10% polarization loss due to this spin direction mismatch. This could be solved with appropriate spin rotators in the injection and extraction beam lines. However, a single additional partial snake located in the synchrotron can provide the spin direction matching at injection and extraction and also increase the effective partial snake strength if its position is chosen properly.

The location and the precession axis direction of multiple partial snakes has to be chosen very carefully to maintain control of the spin tune in a similar way as is necessary for multiple full snakes. For practical partial snakes the precession axis direction is always very close to longitudinal, which leaves only the location and strength of the partial snakes as free parameters.

The spin tune for two partial snakes separated by the fraction $1/m$ of the ring circumference is given by Roser et al. [23]:

$$\cos \pi \nu_{sp} = \cos \frac{s_1 \pi}{2} \cos \frac{s_2 \pi}{2} \cos G\gamma \pi - \sin \frac{s_1 \pi}{2} \sin \frac{s_2 \pi}{2} \cos \frac{G\gamma \pi (m-2)}{m}, \tag{5.25}$$

where $s_1\pi$ and $s_2\pi$ are the rotation angles of the two partial snakes. The derivation is similar to the one partial snake case by using OTM method.

Separating the two partial snakes by one third of the ring is of particular interest since it will introduce a periodicity of three units in the spin tune dependence on $G\gamma$. Since both the super-periodicity of the AGS (12) and the vertical betatron tune ($\sim$9) are divisible by three, the spin tune will be the same at all strong intrinsic resonances, namely $\nu_{sp} = (s_1 + s_2)/2$ for $G\gamma = 3n$, where n is an integer. With both snakes at equal strength s, $\nu_{sp} = s$ they effectively double the strength of one partial snake. At the injection and extraction energies, for which $G\gamma = 3n + 1.5$, the two partial snakes cancel. The polarization direction in the AGS is therefore exactly vertical and no polarization is lost due to spin direction mismatch.

Even using the 10% partial snake together with the presently installed warm helical partial snake with a rotation angle of 10.6° (5.9%) at extraction energy, a very substantial reduction of the injection and extraction spin mismatch can be achieved. At the same time the effective strength of the partial snakes at the strong intrinsic resonances is significantly increased. Since it is not practical to ramp the two partial snake magnets, their fields are kept constant. The snake strength quoted here is the strength at extraction energy. Figure 5.19 shows the spin tune and the vertical betatron tune in the AGS with two partial snakes of 2.11 T (10% partial snake) and 1.53 T (5.9% partial snake), respectively. The partial snakes have to be located as shown in Fig. 5.20, spaced one third of the ring apart. In this case the polarization loss due to injection and extraction mismatch is about 1%. For a single partial snake with strength of 15.9%, the loss would be 6%.

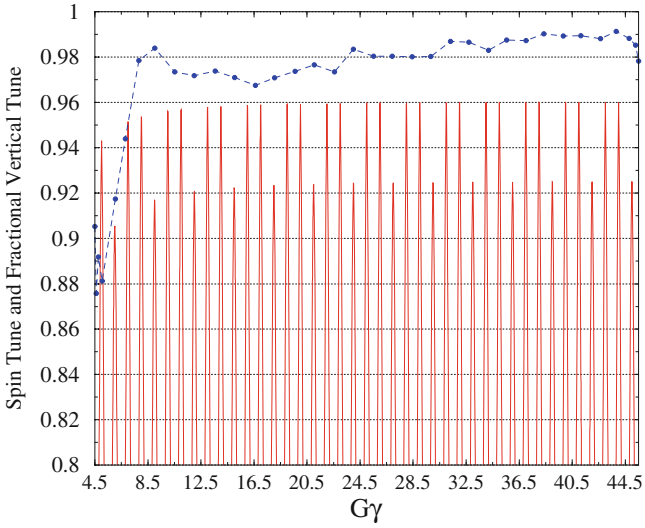

Fig. 5.19 Fractional part of measured vertical tune (dots connected with dashed line) along the energy ramp and spin tune for the combination of 2.11 T and 1.53 T partial snakes

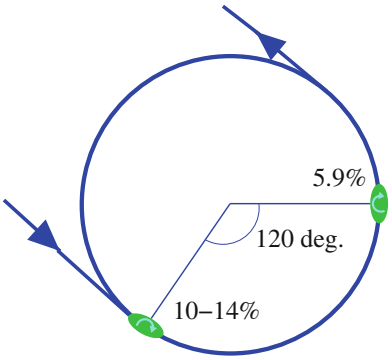

Fig. 5.20 Locations of the partial snakes and the injection and extraction regions that give minimum polarization loss due to spin direction mismatch

To maintain polarization in the AGS, the vertical tunes along the energy ramp have to be put into the spin tune gap generated by the two partial snakes. Moreover, due to the so-called partial snake resonances[14], the available tune space is reduced even further. The partial snake resonances occur when

$$\nu_{sp} = k \pm l\nu_y, \tag{5.26}$$

where k and $l(> 1)$ are integers. This is the same condition as for full snake resonances [24, 25]. The polarization was measured as a function of the vertical

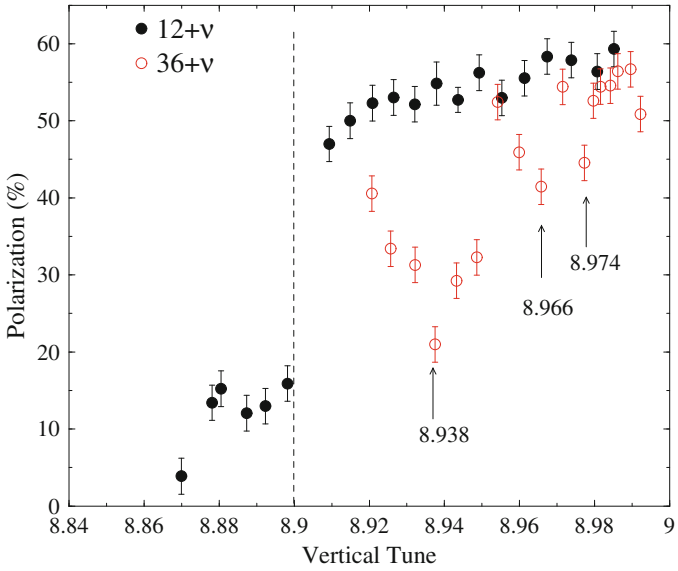

Fig. 5.21 Polarization as function of vertical tunes at two intrinsic resonances with different resonance strength.The dash line shows the position of the spin tune gap for a combined 19.9% (14% + 5.9%) partial snake strength.The locations of high order (l = 2, 3 and 4) snake resonances near intrinsic resonance $36 + \nu_y$ are marked

betatron tune in the vicinity of several intrinsic resonances. Figure 5.21 depicts the effect of the partial snake resonances near the two intrinsic resonances for the 14% cold partial snake and 5.9% warm partial snake. Similar structure has also been observed in the earlier experiment with single partial snake in Fig. 5.18. The high order snake resonance locations can be calculated by solving Eqs. (5.25) and (5.26) and they agree well with the measured values as marked in Fig. 5.21 [26]. The snake resonance strength is proportional to the strength of the nearby intrinsic resonance. The intrinsic resonance strength can be calculated from DEPOL [1] for a given lattice. For the weak intrinsic resonance $(12 + \nu_y)$, there is only a benign effect from the snake resonances and polarization reaches a plateau above 8.96. For the strong intrinsic resonance $(36 + \nu_y)$, the data shows the effect from the second, third and forth order partial snake resonances. The vertical chromaticity was set close to zero along the energy ramp to reduce the betatron tune spread due to the momentum spread. This helps to reduce the depolarization from the snake resonances. As expected, the higher the resonance order, the weaker the resonance strength shown as less of a polarization dip. In addition, when the vertical tune is pushed beyond 8.99, the associated large orbit distortions (see discussion after Eq. (5.27) is likely the cause of the polarization drop of the last data point.

In a synchrotron, the vertical rms closed orbit is given by

$$y_{\mathrm{co,rms}} \approx \frac{\beta_{\mathrm{av}}}{2\sqrt{2} \mid \sin \pi \nu_y \mid} \sqrt{N} \theta_{\mathrm{rms}}, \tag{5.27}$$

where β_{av}, N, ν_y, and θ_{rms} are respectively the average vertical β-function, the number of dipoles with field errors, the vertical betatron tune and the rms steering errors. As seen from Eq. (5.27), the closed orbit amplitude is greatly enhanced when the betatron tune is close to an integer for the same steering errors. As the imperfection resonance strength is proportional to the closed orbit amplitude and beam energy, the imperfection resonance can still be important at high energies even with two partial snakes installed. Since the betatron tune is close to 9, the 9th and multiple of 9 harmonics are strong. The strength of the imperfection resonance calculated for AGS lattice with a large orbit distortion and vertical tune close to 9 could be comparable to the partial snake strength. If they have opposite phase, the imperfection resonance just cancels the effect of the two partial snakes. In fact, we observed polarization loss when the amplitudes of the 9th harmonic of the closed orbit are large. A measurement of polarization as a function of the 9th harmonic orbit amplitude is shown in Fig. 5.22. The depolarization occurs at the expected amplitude.

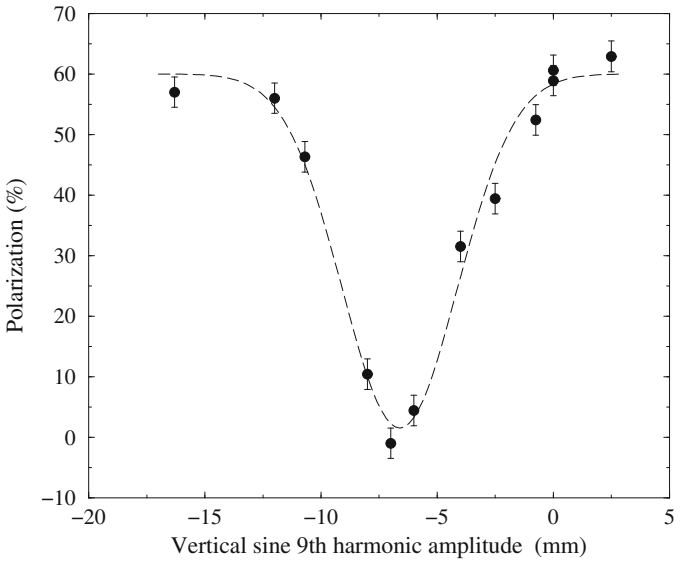

Fig. 5.22 Measured polarization as a function of the sine 9th harmonic amplitude at 36+ν_y. The dashed line is to guide the eyes. The location of the polarization dip agrees with calculation

5.4 Spin Manipulations

5.4.1 Spin Flipper

In polarized proton collision experiments, it is highly advantageous to flip the spin of each bunch of protons during the stores to reduce the systematic errors. The Froissart-Stora formula shows that an artificial resonance can be introduced to flip the spin.

The traditional spin flipping technique uses a single rf spin rotator that rotates the spin around an axis in the horizontal plane. The spin rotator can be implemented as a dipole or a solenoid running with certain rf frequency. It can be done by ramping the frequency of the spin rotator tune ν_{osc} across the spin tune ν_{sp} adiabatically and the spin can be flipped following the Froissart-Stora formula:

$$\frac{P_f}{P_i} = 2\exp[-\frac{\pi}{2}\frac{|\epsilon|^2}{\alpha}] - 1, \tag{5.28}$$

where

$$\alpha = \frac{\Delta\nu_{osc}}{2\pi N} \tag{5.29}$$

where $\Delta\nu_{osc}$ is the range of the rf spin rotator tune sweep range, N is the number of turns the sweep covers. As long as the spin tune is covered by the sweeping range of the rf device, a resonance will be crossed. With proper sweeping speed, the spin can be flipped. Simulations of such a process is shown in Figs. 5.23 and 5.24.

Experiments done at low energies (from 100 MeV to 2 GeV) have demonstrated a spin flip efficiency over 99% [27, 28]. The spin flip is achieved by ramping the rf

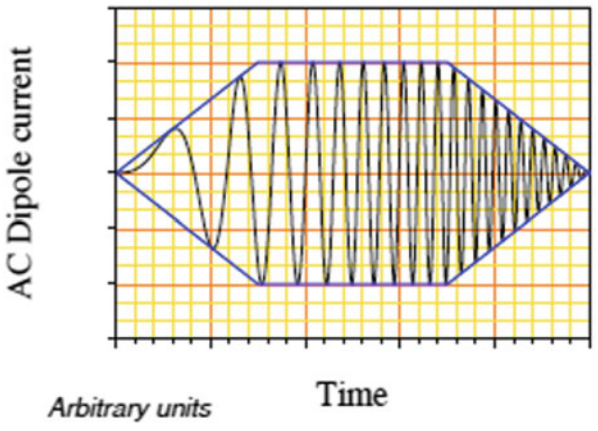

Fig. 5.23 The AC dipole running with frequency sweeping over time

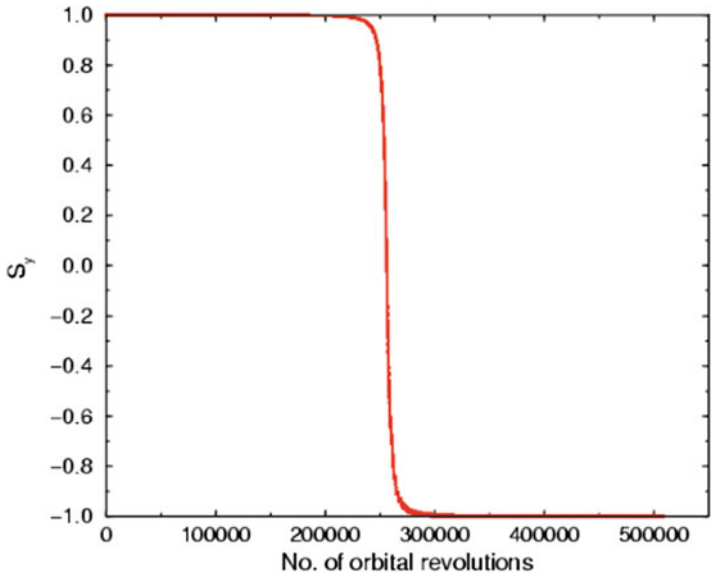

Fig. 5.24 Simulations of spin of an ensemble beam particles in the presence of the artificial resonance from a sweeping AC dipole

spin rotator tune ν_{osc} across the spin tune ν_{sp} adiabatically. The experimental results are shown in Fig. 5.25.

It should be noted that such a single spin rotator generates two spin resonances, one at $\nu_{sp} = \nu_{osc}$, and one at $\nu_{sp} = 1 - \nu_{osc}$ or the so-called "mirror" resonance. As long as the spin tune is sufficiently far away from half integer, say at 0.47, then the two spin resonances are sufficiently far from each other and each one can be treated as an isolated resonance. This is the case for low energies when Siberian Snakes are not needed and the spin tune is not at or near half integer. In high energy polarized proton colliders such as RHIC, the spin tune is very close to half integer. The two spin resonances overlap and their interference makes the full spin flip impossible with such a single rf spin rotator. To reach a full spin flip, the "mirror" resonance has to be eliminated [29].

For the spin flipper to work with a spin tune near 0.5 it has to induce only one spin resonance at $\nu_{sp} = \nu_{osc}$. In addition, it is critical to eliminate any global vertical betatron oscillations driven by the AC dipole to achieve full spin flip [30]. Thus we have chosen a spin flipper design which consists of five AC dipoles with horizontal magnetic field and four DC dipoles with vertical magnetic field, which not only eliminates the "mirror" resonance, but also forms two closed vertical orbital bumps and eliminates the global vertical oscillations outside the spin flipper [31]. Figure 5.26 shows the schematic drawing of the spin flipper design. The first three AC dipoles form the first closed orbital bump and the last three AC dipoles form the second closed orbital bump. The middle AC dipole (No. 3) is used twice. The four

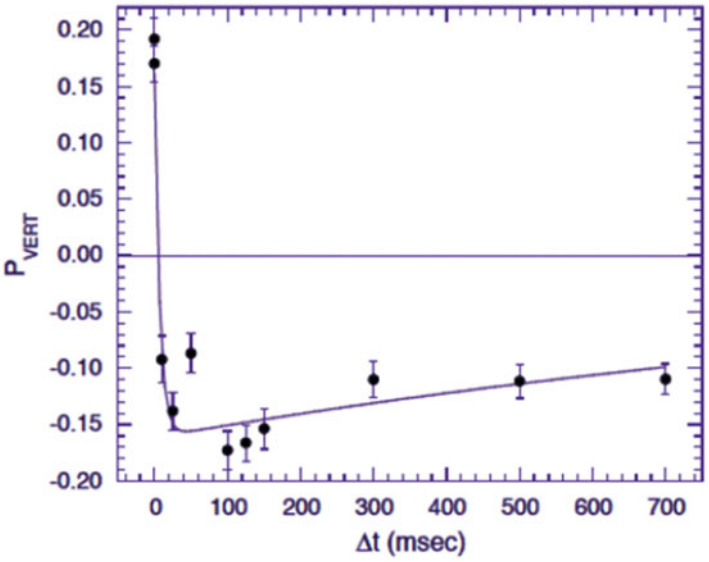

Fig. 5.25 The vertical polarization as a function of the flip time. When the flip time is long enough to satisfy the adiabatic condition, the spin is flipped

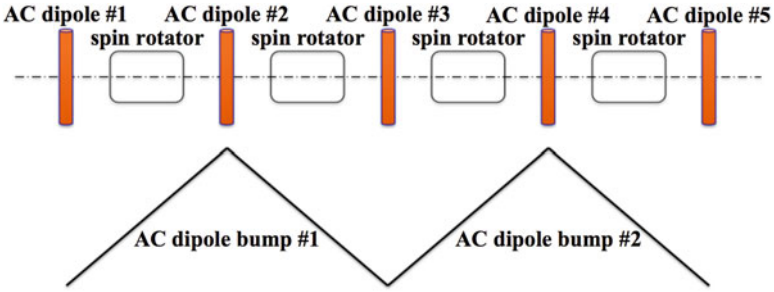

Fig. 5.26 Schematics of the high energy spin flipper in RHIC. It consists of five AC dipoles and four DC dipoles

DC dipoles yield spin rotation angles of $+\psi_0/-\psi_0/-\psi_0/+\psi_0$. The rotation angle ψ_0 is given by

$$\psi_0 = (1 + G\gamma)\frac{B_{dc}L}{B\rho} \tag{5.30}$$

where $B\rho$ is the beam particle magnetic rigidity, $B_{dc}L$ is the integrated B field of each DC dipole. These DC dipoles create a closed local horizontal bump leaving the spin tune ν_{sp} unchanged. The five AC dipoles are operated at the frequency about half of revolution frequency, so that the tune ν_{osc} is in the vicinity of ν_{sp}. AC

dipoles 1–3 and AC dipoles 3–5 create a local vertical orbit bump with a $+\phi_{osc}/-2$ $\phi_{osc}/+\phi_{osc}$ spin rotation sequence. The rotation angle ϕ_{osc} is given by

$$\phi_{osc} = (1 + G\gamma)\frac{B_{ac}l}{B\rho} \tag{5.31}$$

where $B_{ac}l$ is the integrated B field of AC dipole. This configuration induces a spin resonance at $\nu_{osc} = \nu_{sp}$ while eliminating the "mirror" resonance at $1 - \nu_{sp}$ and therefore ensuring a single resonance crossing during a ν_{osc} sweep through $\nu_{sp} \approx \frac{1}{2}$ and producing full spin flip. In the presence of a "mirror" resonance, the isolated resonance crossing condition would otherwise require ν_{sp} to be far enough away from $\frac{1}{2}$. The effective spin resonance strength of the spin flipper ϵ_k then becomes

$$\epsilon_k = 2\frac{\phi_{osc}}{\pi}\sin\psi_0 \sin\frac{\psi_0}{2} \tag{5.32}$$

In order to eliminate the global AC dipole driven vertical betatron oscillations, the currents of the five AC dipoles have to satisfy Eq. (5.33) so that they excite only two closed vertical orbit bumps:

$$\begin{aligned} I_2 &= I_0 \sin(2\pi\nu_{osc}i + \chi_1) \\ I_4 &= I_0 \sin(2\pi\nu_{osc}i + \chi_2) \\ I_1 &= \frac{1}{2}I_0 \sin(2\pi\nu_{osc}i + \chi_1 + \pi) \\ I_5 &= \frac{1}{2}I_0 \sin(2\pi\nu_{osc}i + \chi_2 + \pi) \\ I_3 &= I_1 + I_5 \end{aligned} \tag{5.33}$$

where I_k is the current of k_{th} AC dipole and i is the i_{th} orbital revolution. χ_1 and χ_2 correspond to the initial phase of AC dipole bump 1 and 2, respectively. $\chi_1 - \chi_2 = \psi_0$ is the condition for exciting a single isolated resonance at $\nu_{sp} = \nu_{osc}$ with the spin flipper.

Besides eliminating the "mirror" resonance and any global vertical betatron oscillation driven by AC dipoles, the reduction of the spin tune spread is also critical for achieving full spin flip. The spin tune of a synchrotron with two Siberian Snakes installed at opposite sides of the ring is given by

$$\nu_{sp} = \frac{1}{2} + \frac{(1 + G\gamma)(\theta_1 - \theta_2)}{2\pi}, \tag{5.34}$$

where θ_1 and θ_2 are the integrated bending angles of the first half arc and second half arc, respectively. For the on-energy and on-axis protons both θ_1 and θ_2 are equal (π) and the design-orbit spin tune is $\frac{1}{2}$ independent of the beam energy. This changes when synchrotron motion and the resulting momentum spread $\frac{\Delta p}{p}$ are considered. The change in the bending angles are $\Delta\theta_1 = (x_1' - x_2')$ and $\Delta\theta_2 = (x_2' - x_1')$ respectively, where x_1' and x_2' are the slopes of the beam trajectory at the first and the second Siberian Snake. The spin tune then becomes $\frac{1}{2}+(1+G\gamma)(x_2'-x_1')/\pi$. To the first order, x' can be expressed as $x' = D'\frac{\Delta p}{p}$, which measures orbit difference due to the momentum offset. Here D' is the slope of the dispersion function D, which measures orbit difference due to momentum offset. The momentum spread causes a spin tune spread when the dispersion slopes are different at the two Siberian Snakes [32]:

$$\Delta\nu_{sp} = \frac{(1+G\gamma)}{\pi}(D_1' - D_2')\frac{\Delta p}{p} \tag{5.35}$$

In RHIC, this local dispersion slope difference between the two Siberian Snakes is about 0.045 at 255 GeV, which corresponds to 0.007 spin tune spread for a beam with a momentum spread of 0.001. This is comparable to the proposed spin tune sweep range of 0.02. Hence, successful full spin flipping requires to match the dispersion slopes. Since the $G\gamma$ values of 24 GeV ($G\gamma = 45.5$) and 255 GeV ($G\gamma = 487$) differ by a factor of ten, the required $\Delta D' = (D_1' - D_2')$ is ten times smaller at 255 GeV than at 24 GeV to maintain the same spin tune spread $\Delta\nu_{sp}$. Such a small $\Delta D'$ lattice was achieved by using γ_{tr} transition jump quads [33].

In sweep measurements, the driving tune was swept over typical 0.005 range for a certain time (such as 1 second). The polarization was measured before and after each sweep. At injection, the final to initial polarization ratio was measured with $\Delta D'$ as low as 0.003. The spin flipper was set to sweep from 0.4995 to 0.5045 and the spin tune was 0.5025. The final to initial polarization ratio was measured as function of $\Delta D'$ and the results are shown in Fig. 5.27. The spin flipper sweep time was fixed as 3 seconds during these measurements. It clearly demonstrates that the $\Delta D'$ suppression is critical to achieve a high spin flip efficiency. For a normal lattice where the $\Delta D'$ was large, the polarization was lost with a single spin flipper sweep.

With the 0.005 tune sweep range and the given spin flipper strength, a 99% spin flip efficiency is predicted for a sweep time of 0.6 second or longer at 24 GeV from Eq. (5.28) and numerical simulations [34]. The final to initial polarization ratio from Eq. (5.28) for the given spin flipper strength at injection is plotted in Fig. 5.28 as solid line. But this is an over-simplified model. In reality, the synchrotron motion and residual spin tune spread can have an impact on the final spin flip efficiency. The measured spin flip efficiencies for three different sweep times are also shown in Fig. 5.28 [35]. Each efficiency is the average of 10 to 12 spin flip measurements. The best final to initial polarization ratio $-97.5 \pm 1.9\%$ was obtained with a 1 second sweep time . This is close to the simple model prediction of -99%. At 0.5 second, the final to initial polarization ratio is expected to be slightly worse due

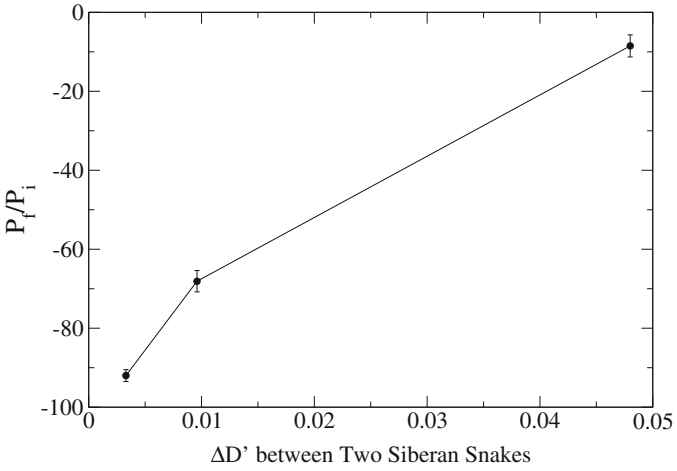

Fig. 5.27 The average final to initial polarization ratio for 3 seconds sweep time at injection as function of ΔD' at the two Siberian Snakes. The small $\Delta D'$ is critical for full spin flip

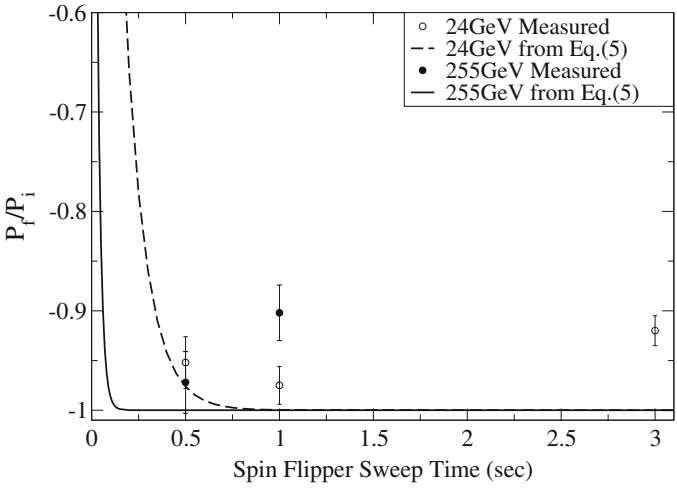

Fig. 5.28 The average final to initial polarization ratio at 24 GeV and 255 GeV. The solid line is the polarization flip ratio from Eq. (5.28) for the resonance strength 0.00024 and the filled points are the averaged spin flip efficiencies for three different sweep times at 24 GeV. The dashed line and open points are for 255 GeV and the resonance strength 0.00057

to faster crossing speed, and the measured value $-95 \pm 2.6\%$ is indeed slightly smaller. For the slowest sweep time, 3 seconds, the final to initial polarization ratio is only $-92.0 \pm 1.5\%$. There are several reasons for this. First, with a slower sweep speed, multiple spin resonance crossings with different resonance crossing speeds can happen due to the synchrotron oscillation. Second, the polarization loss from

weak higher order depolarizing resonances would be enhanced with a slow sweep speed.

The final to initial polarization ratio obtained from the given spin flipper strength at 255 GeV is plotted in Fig. 5.28 as dashed line. The spin flip efficiencies for the two different sweep times are also shown in Fig. 5.28. As before, each efficiency is the average of 10 to 12 spin flip measurements. The better final to initial polarization ratio $-97.2 \pm 3.1\%$ was obtained at the 0.5 second sweep time. This is close to the simple model prediction of -99%. For the slower sweep time of 1 second the final to initial polarization ratio is $-90.2 \pm 2.8\%$. Similar to the 24 GeV case, the final to initial polarization ratio is worse with slow sweep speed.

5.4.2 Spin Tune Measurement

In principle, the spin tune can be measured with a similar idea as the betatron tune measurement: measuring the spin response to a driven spin coherence. Such a method can also be non-destructive. A coherent spin precession around the vertical direction can be adiabatically induced by driving the AC spin rotator at a drive tune near the spin tune.

If the undisturbed stable spin direction on the designed orbit is vertical, the vertical component of polarization P in the neighborhood of an isolated spin resonance is given by Lee [20] and Bai and Roser [29]:

$$P_y = \frac{\nu_{\mathrm{sp}} - \nu_{\mathrm{osc}}}{\sqrt{|\nu_{\mathrm{sp}} - \nu_{\mathrm{osc}}|^2 + |\epsilon|^2}}\,, \tag{5.36}$$

where ϵ is the strength of the driven spin resonance and ν_{osc} is the drive tune. The horizontal component oscillates with ν_{osc}:

$$P_x = \frac{|\epsilon|}{\sqrt{|\nu_{\mathrm{sp}} - \nu_{\mathrm{osc}}|^2 + |\epsilon|^2}} \cos(2\pi\,\nu_{\mathrm{osc}} i - \Psi)\,, \tag{5.37}$$

where i is the ith orbital revolution and Ψ is the initial phase offset. Equations (5.36) and (5.37) describe the vertical and horizontal components in a perfect accelerator in the presence of a single isolated spin resonance. The ratio of $\hat{P}_x$ and P_y gives the difference between ν_s and ν_{osc}:

$$\tan\theta_0 = \frac{\hat{P}_x}{P_y} = \frac{|\epsilon|}{\nu_s - \nu_{\mathrm{osc}}}\,, \tag{5.38}$$

where θ_0 is the opening angle of the polarization vector. With the known resonance strength ϵ from the spin flipper and the drive tune ν_{osc}, the spin tune ν_{sp} can be derived from the measured quantity $\tan\theta_0$.

This technique has two advantages. First, it is an adiabatic spin manipulation and preserves the beam polarization. Second, it is a relatively fast measurement. Hence, this technique is ideal for measuring the spin tune at the store energy of a high-energy polarized synchrotron, such as RHIC or a future polarized electron ion collider [36]. The spin tune measurement with coherent spin motion has been used for deuteron beams [37] at low energy (∼1 GeV) in COSY, although the coherent spin motion was not driven. Here the first spin tune measurement at high energies (24 and 255 GeV) for protons in RHIC using a driven coherent spin motion will be discussed as examples [38].

The focus of this experiment is to measure θ_{sp}, the azimuthal angle of the spin vector in the plane transverse to the beam moving direction, and understand how it is influenced by the coherent spin motion. To measure the driven coherent spin motion, recoil carbon events from the proton-carbon (pC) polarimeter [39] need to be recorded on a turn-by-turn basis. The polarimeter related information can be found in Chap. 12 for the hadron polarimeter. Figure 5.29 shows the spin precession projected onto the x-y plane transverse to the beam direction. The pC polarimeter measures the spin vector projection in this plane. With a driven coherent spin motion the spin vector in this plane oscillates over the range shown by the two dashed arrows, with a period equal to that of the driven resonance. The amplitude of the precession is θ_0 from Eq. (5.38); θ_{tilt} is an arbitrary offset between vertical and the stable spin direction. From $\hat{P}_x/P_y$ the spin azimuthal angle θ_{sp} measured by the pC polarimeter with a possible tilt angle θ_{tilt} will follow the precession

$$\frac{\hat{P}_x}{P_y} = \tan(\theta_{sp} - \theta_{\text{tilt}}) = \tan\theta_0 \cos(2\pi\nu_{\text{osc}} i - \Psi)\,. \tag{5.39}$$

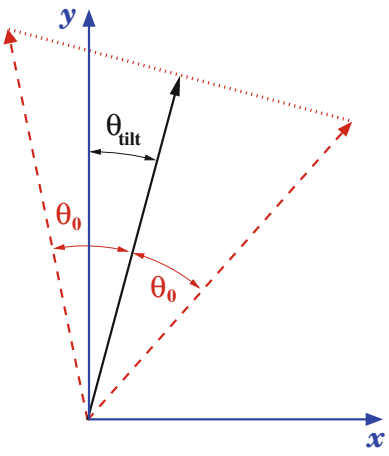

Fig. 5.29 Projection of the spin vector into the transverse plane when the spin tune is near a spin resonance. The spin oscillates around the stable spin direction (solid arrow) between the two boundaries (dashed arrows) over many orbit turns

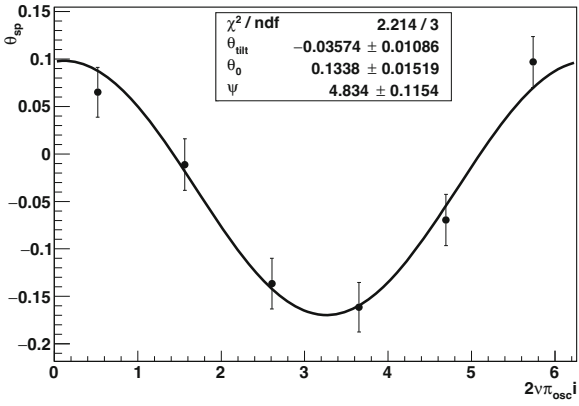

Fig. 5.30 Measured spin azimuthal angle as a function of the driven oscillation phase at 24 GeV with drive tune as 0.498. All angles (θ_{sp}, θ_{tilt}, θ_0, Ψ) are in the unit of radian. The nonzero θ_{tilt} means that the stable spin direction is tilted away from vertical

Note that only the two transverse components of the polarization can be measured. If the spin direction has a significant longitudinal component in addition to the angle θ_{tilt}, the simple form of Eq. (5.39) should be modified.

The experiment was carried out at injection energy of 24 GeV and the store energy of 255 GeV. The revolution frequency in RHIC is about 78.20 kHz. The bunch pattern was 120 bunches in the ring and RHIC bunch crossings were used as a clock signal for the analysis. For these measurements, a signal from the resonance drive was provided to the polarimeter readout, which allowed the alignment of the phase of carbon hits within one period of the resonance drive. The drive signal was read with an accuracy of two bunch crossings, whereas the typical period of the drive was ∼240 bunch crossings (for a drive tune near 0.5), so the phase of carbon hits was known to within 1% of a period.

Figure 5.30 shows θ_{sp} versus one cycle of drive phase for one drive setting. To improve the statistical accuracy, the carbon hits were grouped in six bins of 40 bunch crossings, spanning nearly one entire drive cycle; the mean spin azimuthal angle θ_{sp} was measured for each bin. The curve is fit to the function, from rearrangement of Eq. (5.39):

$$\theta_{sp}(i) = \theta_{\text{tilt}} + \tan^{-1}[\tan\theta_0 \cos(2\pi\,\nu_{\text{osc}} i - \Psi)]\,. \tag{5.40}$$

The arbitrary phase offset Ψ depends on the propagation time of proton bunches from the drive to the polarimeter, and the cable delay of the signal from the drive to the polarimeter readout. With the measured $\theta_0 = 0.1338 \pm 0.01519$ and the driving tune at 0.498, the spin tune can be derived from Eq. (5.38) as 0.4998 ± 0.0002, fairly close to 0.5.

Driven coherent spin motion has been used to measure the spin tune in RHIC at 24 and 255 GeV. The results show that the spin tune can be measured by driven spin coherence when the tune separation is small enough. The drive tune needs to be close to the spin tune, which requires a small spin tune spread. In RHIC, where a pair of Siberian snakes are used, the small spin tune spread was achieved by the

reduction of the dispersion slope difference at the two Siberian snakes [32, 33]. These experimental results prove that it is possible to routinely measure the spin tune of polarized proton beams—the most important polarized beam parameter. This will lead to more stable and optimized operations of a high-energy polarized collider, such as RHIC or a future polarized electron ion collider.

5.5 Summary

The preservation of polarization through the acceleration can be divided into two big categories. The first one is to reduce or eliminate the effect of spin resonances. Harmonic orbit correction, fast acceleration, radial jump, tune jump and full snake are the mechanisms that can be applied in this category. Among them, the harmonic orbit correction could be tedious if many are needed. The fast tune jump could lead to a emittance growth as this is a non-adiabatic operation. The full snake eliminates the resonance condition completely but the higher order resonances called snake resonances are still present which requires special optical design to avoid and mitigate them. The second category is to enhance the resonance strength. AC dipole, partial snake (weak or strong) are in this category. An AC dipole requires a large machine aperture and/or reasonable strong resonance strengths to overcome intrinsic resonances, which in reality can not always be met. Most of these methods are based on the Froissart-Stora formula. This formula is also the basis of spin manipulation in a synchrotron. The examples of spin flip and spin tune measurement were presented and discussed.

5.6 Homework

? Exercise 1: Polarization of a Gaussian Beam

For a Gaussian distribution, derive the Froissart-Stora formula for the whole beam, namely, Eq. (5.3).

Solution
In the integrand of $< P_f/P_i >$, Eq. (5.1):

- substitute the expression for the density $\rho(\varepsilon)$ (Eq. (5.1), right hand side),
- substitute the expression for the strength $|\epsilon(\varepsilon)|$ (Eq. (5.2)).

Equation (5.1) can thus be recast under the form

$$< P_f/P_i > = \int_0^\infty \exp\frac{-\varepsilon}{2\varepsilon_0}\left(1+\frac{\pi|\epsilon(\varepsilon_0)|^2}{\alpha}\right)\frac{d\varepsilon}{\varepsilon_0} - \underbrace{\int_0^\infty \rho(\varepsilon)\,d\varepsilon}_{=1}$$

Introduce the change of variable $\frac{\varepsilon}{2\varepsilon_0}(1+\frac{\pi|\epsilon(\varepsilon_0)|^2}{\alpha}) = x$, then $\frac{d\varepsilon}{\varepsilon_0} = \frac{2}{1+\frac{\pi|\epsilon(\varepsilon_0)|^2}{\alpha}}dx$. Substituting into the integral above gives the expected result:

$$< P_f/P_i >= \frac{2}{1+\frac{\pi|\epsilon(\varepsilon_0)|^2}{\alpha}}\int_0^\infty e^{-x}dx - 1 = \frac{1-\frac{\pi|\epsilon(\varepsilon_0)|^2}{\alpha}}{1+\frac{\pi|\epsilon(\varepsilon_0)|^2}{\alpha}}$$

? Exercise 2: Harmonic Orbit Correction, Experimental Data

Tables 5.1 and 5.2 provide the experimental data from a scan of the vertical third harmonics (the cos3v and sin3v components of the vertical closed orbit) in the AGS Booster. The polarization is given in an arbitrary unit. Actually, it is called asymmetry and needs to be divided by the so-called analyzing power to give a polarization value between -1 and $+1$. Use the Eq. (5.6) to fit these data. The exercise is to find the corrector current value I_0 (*i.e.*, I_{c0} and I_{s0} for respectively the cosine and sine corrector families) to be used for a full correction of the third orbit harmonic. For this purpose, we don't care about the unit of the polarization. There are three parameters for the data fitting (Eq. (5.7)): P_i, I_0 and σ. Among the three parameters, I_0 is the most important one and σ provides sensitivity of the polarization to the variation of the particular harmonic component. If possible, plot the fitted curve and experiment data together on one plot.

Solution

The harmonic scan data need to be fitted with the following equation for the sine and cosine components (see Eqs. (5.6) and (5.7)):

$$P_f = p_0\left(2\exp\frac{-\pi(I-p_1)^2}{2p_2^2} - p_3\right)$$

The fitting results are shown in Figs. 5.31 and 5.32. The experimental data of sin3v was taken first followed by cos3v data taking. The optimized sin3v setting was put in before cos3v scan. As one can see, the parameter p_3 (Eq. (5.7)) in the cos3v fitting is close to 1 as expected.

Note that since the p_0 and p_3 parameters are correlated, one can get different sets of p_0 and p_3 from the fitting.

Table 5.1 3rd harmonic sine current scan

cos3v I (A)	Asymmetry	Error bar
10	270.471	4.096
9	187.052	4.719
8	123.548	4.211
7	40.727	4.15
6	−39.088	4.184
5	−124.047	4.225
4	−205.082	4.084
3	−303.959	5.397
2	−374.321	4.215
1	−438.749	4.064
0	−510.413	4.076
−1	−579.386	4.07
−2	−628.054	4.051
−3	−676.508	4.087
−4	−701.441	4.121
−5	−727.928	4.312
−6	−730.051	4.902
−7	−733.544	4.089
−8	−719.381	4.495
−9	−683.714	4.318
−10	−626.98	4.124
−11	−578.39	4.194
−12	−523.706	4.167
−13	−454.92	4.242

Table 5.2 3rd harmonic cosine current scan

sin3v I (A)	Asymmetry	Error bar
5.2	−164.591	3.963
4.2	−297.504	4.098
3.2	−438.518	3.999
2.2	−569.737	4.015
1.2	−672.803	4.032
0.2	−719.652	3.988
−0.8	−756.134	4.035
−1.8	−737.453	4.095
−2.8	−694.489	4.086
−3.8	−595.165	4.006
−4.8	−481.373	4.162

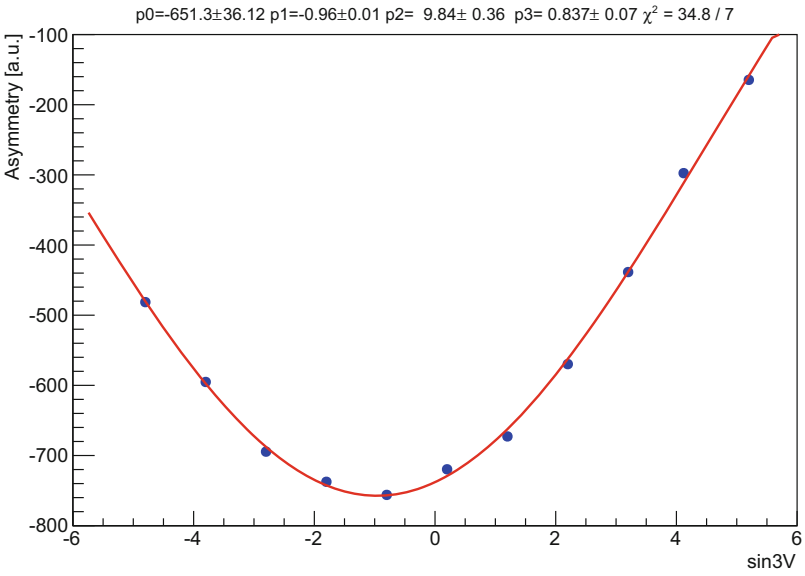

Fig. 5.31 The fitting results for sin3v data. The fitting parameter values are given at the top of the plot

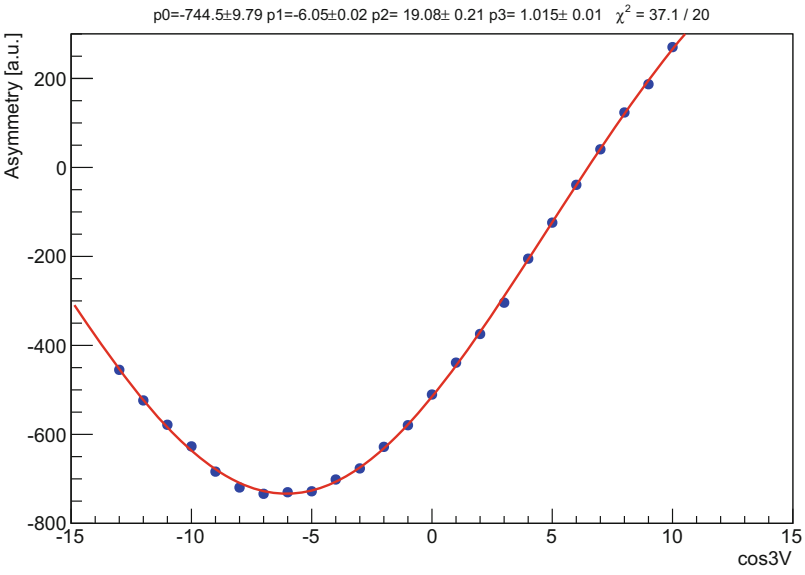

Fig. 5.32 The fitting results for cos3v data. The fitting parameter values are given at the top of the plot

References

1. E.D. Courant, R.D. Ruth, BNL Report 51270 (1980)
2. M. Froissart, R. Stora, Nucl. Instrum. Methods Phys. Res. **7**, 297 (1960)
3. F.Z. Khiari et al., Phys. Rev. D **39**, 45 (1989)
4. H. Sato et al., Nucl. Instrum. Methods **A272**, 617 (1988); H. Sato et al., IEEE Transaction NS-32, 1950 (1985); H. Sato et al., Proc. PAC **89**, 1758 (1989).
5. E. Gorud et al., AIP Conf. Proc. **95**, 407 (1982)
6. A. Lehrach et al., in *Proceedings of the SPIN96* (World Scientific, Singapore, 1997), p. 416
7. H. Huang et al., in *Proceedings of the SPIN96* (World Scientific, Singapore, 1997), p. 528
8. A. Lehrach et al., Nucl. Instrum. Methods **A439**, 26 (2000)
9. L.A. Ahrens et al., AIP Conf. Proc. **187**, 1068 (1988)
10. F. Lin et al., Phys. Rev. ST Accel. Beams **10**, 044001 (2007)
11. H. Huang et al., Phys. Rev. ST Accel. Beams **14**, 081001 (2014)
12. H. Huang et al., Phys. Rev. ST Accel. Beams **23**, 021001 (2020)
13. V.H. Ranjbar et al., Phys. Rev. Accel. Beams **21**, 111003 (2018)
14. S.Y. Lee and S. Tepikian, Phys. Rev. Lett. **56**, 1635 (1986)
15. M. Bai et al., Phys. Rev. Lett. **96**, 174801 (2006)
16. Y.S. Derbenev, University of Michigan report UM HE 96-05 (1996)
17. D.D. Caussyn et al., Phys. Rev. Lett. **73**, 2857 (1994)
18. M. Bai et al., Phys. Rev. Lett. **80**, 4673 (1998)
19. T. Roser, in *Proceedings of the 8th International Symposium on High-Energy Spin Physics, Minneapolis, 1988, AIP Conference Proceedings No 187* (AIP, New York, 1989), p. 1442
20. S.Y. Lee, *Spin Dynamics and Snakes in Synchrotrons* (World Scientific, Singapore, 1997)
21. H. Huang et al., Phys. Rev. Lett. **73**, 2982 (1994)
22. H. Huang et al., Phys. Rev. ST Accel. Beams **7**, 071001 (2004)
23. T. Roser et al., in *Proceedings of the EPAC04* (2004), p. 1577
24. R.A. Phelps et al., Phys. Rev. Lett. **78**, 2772 (1997)
25. V.H. Ranjbar et al., Phy. Rev. Lett. **91**, 034801 (2003)
26. H. Huang et al., Phys. Rev. Lett. **99**, 154801 (2007)
27. V.A. Anferov et al., Phys. Rev. ST Accel. Beams **3**, 041001 (2000)
28. M.A. Leonova et al., Phys. Rev. Lett. **93**, 224801 (2004)
29. M. Bai, T. Roser, Phys. Rev. ST Accel. Beams **11**, 091001 (2008)
30. S. Mane, Phys. Rev. ST Accel. Beams **12**, 099001 (2009)
31. M. Bai et al., in *Proceedings of the IPAC 2010* (2010), p. 1224
32. V. Ptitsyn et al., in *Proceedings of the IPAC 2010* (2010), p. 4641
33. C. Liu , J. Kewisch, H. Huang, M. Minty, Phys. Rev. ST Accel. Beams **22**, 061002 (2019)
34. F. Méot et al., BNL C-AD Tech Notes AP 589 (2017) (unpublished)
35. H. Huang et al., Phys. Rev. Lett. **120**, 264804 (2018)
36. A. Accardi et al., Eur. Phys. J. A **52**, 268 (2016)
37. D. Eversmann et al., Phys. Rev. Lett. **115**, 094801 (2015)
38. H. Huang et al., Phys. Rev. Lett. **122**, 204803 (2019)
39. H. Huang, K. Kurita, AIP Proc.**868**, 3 (2006)